
The GAN is dead; long live the GAN!

A Modern Baseline GAN

Yiwen Huang
Brown University

Aaron Gokaslan
Cornell University

Volodymyr Kuleshov
Cornell University

James Tompkin
Brown University

Abstract

There is a widely-spread claim that GANs are difficult to train, and GAN architectures in the literature are littered with empirical tricks. We provide evidence against this claim and build a modern GAN baseline in a more principled manner. First, we derive a well-behaved regularized relativistic GAN loss that addresses issues of mode dropping and non-convergence that were previously tackled via a bag of ad-hoc tricks. We analyze our loss mathematically and prove that it admits local convergence guarantees, unlike most existing relativistic losses. Second, this loss allows us to discard all ad-hoc tricks and replace outdated backbones used in common GANs with modern architectures. Using StyleGAN2 as an example, we present a roadmap of simplification and modernization that results in a new minimalist baseline—R3GAN (“Re-GAN”). Despite being simple, our approach surpasses StyleGAN2 on FFHQ, ImageNet, CIFAR, and Stacked MNIST datasets, and compares favorably against state-of-the-art GANs and diffusion models. Code: <https://www.github.com/brownvc/R3GAN>

1 Introduction

Generative adversarial networks (GANs) let us generate high-quality images in a single forward pass. However, the original objective in Goodfellow *et al.* [13], is notoriously difficult to optimize due to its minimax nature. This leads to a fear that training might diverge at any point due to instability, and a fear that generated images might lose diversity through mode collapse. While there has been progress in GAN objectives [14, 22, 81, 52, 64], practically, the effects of brittle losses are still regularly felt. This notoriety has had a lasting negative impact on GAN research.

A complementary issue—partly motivated by this instability—is that existing popular GAN backbones like StyleGAN [29, 31, 30, 32] use many poorly-understood empirical tricks with little theory. For instance, StyleGAN uses a gradient penalized non-saturating loss [52] to increase stability (affecting sample diversity), but then employs a minibatch standard deviation trick [28] to increase sample diversity. Without tricks, the StyleGAN backbone still resembles DCGAN [60] from 2015, yet it is still the common backbone of SOTA GANs such as GigaGAN [26] and StyleGAN-T [70]. Advances in GANs have been conservative compared to other generative models such as diffusion models [20, 78, 33, 34], where modern computer vision techniques such as multi-headed self attention [87] and backbones such as preactivated ResNet [17], U-Net [63] and vision transformers (ViTs) [9] are the norm. Given outdated backbones, it is not surprising that there is a widely-spread belief that GANs do not scale in terms of quantitative metrics like Frechet Inception Distance [19].

We reconsider this situation: we show that by combining progress in objectives into a regularized training loss, GANs gain improved training stability, which allows us to upgrade GANs with modern backbones. First, we propose a novel objective that augments the relativistic pairing GAN loss (RpGAN; [22]) with zero-centered gradient penalties [52, 64], improving stability [14, 64, 52]. We show mathematically that gradient-penalized RpGAN enjoys the same guarantee of local convergence as regularized classic GANs, and that removing our regularization scheme induces non-convergence.

Once we have a well-behaved loss, none of the GAN tricks are necessary [28, 31], and we are free to engineer a modern SOTA backbone architecture. We strip StyleGAN of all its features, identify those that are essential, then borrow new architecture designs from modern ConvNets and transformers [48, 97]. Briefly, we find that proper ResNet design [17, 67], initialization [99], and resampling [29, 31, 32, 100] are important, along with grouped convolution [95, 5] and no normalization [31, 34, 14, 88, 4]. This leads to a design that is simpler than StyleGAN and improves FID performance for the same network capacity (2.75 vs. 3.78 on FFHQ-256).

In summary, our work first argues mathematically that GANs need not be tricky to train via an improved regularized loss. Then, it empirically develops a simple GAN baseline that, without any tricks, compares favorably by FID to StyleGAN [29, 31, 32], other SOTA GANs [3, 42, 94], and diffusion models [20, 78, 86] across FFHQ, ImageNet, CIFAR, and Stacked MNIST datasets.

2 Serving Two Masters: Stability and Diversity with RpGAN + R_1 + R_2

In defining a GAN objective, we tackle two challenges: stability and diversity. Some previous work deals with stability [29, 31, 32] and other previous work deals with mode collapse [22]. To make progress in both, we combine a stable method with a simple regularizer that is grounded by theory.

2.1 Traditional GAN

A traditional GAN [13, 57] is formulated as a minimax game between a discriminator (or critic) D_ψ and a generator G_θ . Given real data $x \sim p_{\mathcal{D}}$ and fake data $x \sim p_\theta$ produced by G_θ , the most general form of a GAN is given by:

$$\mathcal{L}(\theta, \psi) = \mathbb{E}_{z \sim p_z} [f(D_\psi(G_\theta(z)))] + \mathbb{E}_{x \sim p_{\mathcal{D}}} [f(-D_\psi(x))] \quad (1)$$

where G tries to minimize \mathcal{L} while D tries to maximize it. The choice of f is flexible [50, 44]. In particular, $f(t) = -\log(1 + e^{-t})$ recovers the classic GAN by Goodfellow *et al.* [13]. For the rest of this work, this will be our choice of f [57].

It has been shown that Equation 1 has convex properties when p_θ can be optimized directly [13, 81]. However, in practical implementations, the empirical GAN loss typically shifts fake samples beyond the decision boundary set by D , as opposed to directly updating the density function p_θ . This deviation leads to a significantly more challenging problem, characterized by susceptibility to two prevalent failure scenarios: mode collapse/dropping¹ and non-convergence.

2.2 Relativistic f -GAN

We employ a slightly different minimax game named relativistic pairing GAN (RpGAN) by Jolicoeur-Martineau *et al.* [22] to address mode dropping. The general RpGAN is defined as:

$$\mathcal{L}(\theta, \psi) = \mathbb{E}_{\substack{z \sim p_z \\ x \sim p_{\mathcal{D}}}} [f(D_\psi(G_\theta(z)) - D_\psi(x))] \quad (2)$$

Although Eq. 2 differs only slightly from Eq. 1, evaluating this critic difference has a fundamental impact on the landscape of \mathcal{L} . Since Eq. 1 merely requires D to separate real and fake data, in the scenario where all real and fake data can be separated by a single decision boundary, the empirical GAN loss encourages G to simply move all fake samples barely past this single boundary—this degenerate solution is what we observe as mode collapse/dropping. Sun *et al.* [81] characterize such degenerate solutions as bad local minima in the landscape of \mathcal{L} , and show that Eq. 1 has *exponentially many* bad local minima. The culprit is the existence of a single decision boundary that naturally arises when real and fake data are considered in isolation. RpGAN introduces a simple solution by coupling real and fake data, *i.e.* a fake sample is critiqued by its realness *relative to* a real sample, which effectively maintains a decision boundary in the neighborhood of *each* real sample and hence forbids mode dropping. Sun *et al.* [81] show that the landscape of Eq. 2 contains no local minima that correspond to mode dropping solutions, and that every basin is a global minimum.

¹While mode collapse and mode dropping are technically distinct issues, they are used interchangeably in this context to describe the common problem where $\text{supp}(p_\theta)$ does not comprehensively cover $\text{supp}(p_{\mathcal{D}})$. Mode collapse refers to the generator producing a limited diversity of samples (*i.e.*, one image for the entire distribution), whereas mode dropping involves the generator failing to represent certain modes of the data distribution (ignoring entire subsets of the training distribution).

2.3 Training Dynamics of RpGAN

Although the RpGAN landscape result [81] allows us to address mode dropping, the training dynamics of RpGAN have yet to be studied. The ultimate goal of Eq. 2 is to find the equilibrium (θ^*, ψ^*) such that $p_{\theta^*} = p_{\mathcal{D}}$ and D_{ψ^*} is constant everywhere on $p_{\mathcal{D}}$. Sun *et al.* [81] show that θ^* is globally reachable along a non-increasing trajectory in the landscape of Eq. 2 under reasonable assumptions. However, the existence of such a trajectory does not necessarily mean that gradient descent will find it. Jolicoeur-Martineau *et al.* show empirically that unregularized RpGAN does not perform well [22].

Proposition I. (Informal) *Unregularized RpGAN does not always converge using gradient descent.*

We confirm this proposition with a proof in Appendix B. We show analytically that RpGAN does not converge for certain types of $p_{\mathcal{D}}$, such as ones that approach a delta distribution. Thus, further regularization is necessary to fill in the missing piece of a well-behaved loss.

Zero-centered gradient penalties. To tackle RpGAN non-convergence, we explore gradient penalties as the solution since it is proven that zero-centered gradient penalties (0-GP) facilitate convergent training for classic GANs [52]. The two most commonly-used 0-GPs are R_1 and R_2 :

$$\begin{aligned} R_1(\psi) &= \frac{\gamma}{2} \mathbb{E}_{x \sim p_{\mathcal{D}}} \left[\|\nabla_x D_{\psi}\|^2 \right] \\ R_2(\theta, \psi) &= \frac{\gamma}{2} \mathbb{E}_{x \sim p_{\theta}} \left[\|\nabla_x D_{\psi}\|^2 \right] \end{aligned} \quad (3)$$

R_1 penalizes the gradient norm of D on real data, and R_2 penalizes the gradient norm of D on fake data. Analysis on the training dynamics of GANs has thus far focused on local convergence [55, 51, 52], *i.e.*, whether the training at least converges when (θ, ψ) are in a neighborhood of (θ^*, ψ^*) . In such a scenario, the convergence behavior can be analyzed [55, 51, 52] by examining the spectrum of the Jacobian of the gradient vector field $(-\nabla_{\theta} \mathcal{L}, \nabla_{\psi} \mathcal{L})$ at (θ^*, ψ^*) . The key insight here is that when G already produces the true distribution, we want $\nabla_x D = 0$, so that G is not pushed away from its optimal state, and thus the training does not oscillate. R_1 and R_2 impose such a constraint when $p_{\theta} = p_{\mathcal{D}}$. This also explains why earlier attempts at gradient penalties, such as the one-centered gradient penalty (1-GP) in WGAN-GP [14], fail to achieve convergent training [52] as they still encourage D to have a non-zero slope when G has reached optimality.

Since the same insight also applies to RpGAN, we extend our previous analysis and show that:

Proposition II. (Informal) *RpGAN with R_1 or R_2 regularization is locally convergent subject to similar assumptions as in Mescheder *et al.* [52].*

In Appendix C, our proof similarly analyzes the eigenvalues of the Jacobian of the regularized RpGAN gradient vector field at (θ^*, ψ^*) . We show that all eigenvalues have a negative real part; thus, regularized RpGAN is convergent in a neighborhood of (θ^*, ψ^*) for small enough learning rates [52].

Discussion. Another line of work [64] links R_1 and R_2 to instance noise [75] as its analytical approximation. Roth *et al.* [64] showed that for the classic GAN [13] by Goodfellow *et al.*, R_1 approximates convolving $p_{\mathcal{D}}$ with the density function of $\mathcal{N}(0, \gamma I)$, up to additional weighting and a Laplacian error term. R_2 likewise approximates convolving p_{θ} with $\mathcal{N}(0, \gamma I)$ up to similar error terms. The Laplacian error terms from R_1, R_2 cancel when D_{ψ} approaches D_{ψ^*} . We do not extend Roth *et al.*'s proof [64] to RpGAN; however, this approach might provide complimentary insights to our work, which follows the strategy of Mescheder *et al.* [52].

2.4 A Practical Demonstration

We experiment with how well-behaved our loss is on StackedMNIST [46] which consists of 1000 uniformly-distributed modes. The network is a small ResNet [17] for G and D without any normalization layers [21, 91, 1, 85]. Through the use of a pretrained MNIST classifier, we can explicitly measure how many modes of $p_{\mathcal{D}}$ are recovered by p_{θ} . Furthermore, we can estimate the reverse KL divergence between the fake and real samples $D_{\text{KL}}(p_{\theta} \parallel p_{\mathcal{D}})$ via the KL divergence between the categorical distribution of p_{θ} and the true uniform distribution.

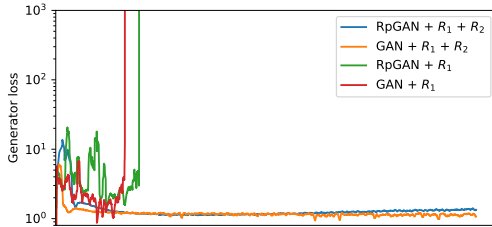


Figure 1: Generator G loss for different objectives over training. Regardless of which objective is used, training diverges with only R_1 and succeeded with both R_1 and R_2 . Convergence failure with only R_1 was noted by Lee et al. [42].

Loss	# modes \uparrow	$D_{\text{KL}}\downarrow$
RpGAN + R_1 + R_2	1000	0.0781
GAN + R_1 + R_2	693	0.9270
RpGAN + R_1	Fail	Fail
GAN + R_1	Fail	Fail

Table 1: StackedMNIST [46] result for each loss function. The maximum possible mode coverage is 1000. “Fail” indicates that training diverged early on.

A conventional GAN loss with R_1 , as used by Mescheder et al. [52] and the StyleGAN series [29, 31, 32], diverges quickly (Fig. 1). Next, while theoretically sufficient for local convergence, RpGAN with only R_1 regularization is also unstable and diverges quickly². In each case, the gradient of D on fake samples explodes when training diverges. With both R_1 and R_2 , training becomes stable for both the classic GAN and RpGAN. Now stable, we can see that the classic GAN suffers from mode dropping, whereas RpGAN achieves full mode coverage (Tab. 1) and reduces D_{KL} from 0.9270 to 0.0781. As a point of contrast, StyleGAN [29, 31, 30, 32] uses the minibatch standard deviation trick to reduce mode dropping, improving mode coverage from 857 to 881 on StackedMNIST³ and with barely any improvement on D_{KL} [28].

R_1 alone is not sufficient for globally-convergent training. While a theoretical analysis of this is difficult, our small demonstration still provides insights into the assumptions of our convergence proof. In particular, the assumption that (θ, ψ) are sufficiently close to (θ^*, ψ^*) is highly unlikely early in training. In this scenario, if D is sufficiently powerful, regularizing D solely on real data is not likely to have much effect on D ’s behavior on fake data and so training can fail due to an ill-behaved D on fake data. This observation has been made by previous studies [84, 83] specifically for empirical GAN training, that regularizing an empirical discriminator with only R_1 leads to gradient explosion on fake data due to the memorization of real samples.

Thus, the practical solution is to regularize D on both real and fake data. The benefit of doing so can be viewed from the insight of Roth et al. [64]: that applying R_1 and R_2 in conjunction smooths both $p_{\mathcal{D}}$ and p_{θ} which makes learning easier than only smoothing $p_{\mathcal{D}}$. We also find empirically that with both R_1 and R_2 in place, D tends to satisfy $\mathbb{E}_{x \sim p_{\mathcal{D}}} [\|\nabla_x D\|^2] \approx \mathbb{E}_{x \sim p_{\theta}} [\|\nabla_x D\|^2]$ even early in the training. Jolicoeur-Martineau et al. [23] show that in this case D becomes a maximum margin classifier—but if only one regularization term is applied, this does not hold. Additionally, having roughly the same gradient norm on real and fake data potentially reduces discriminator overfitting, as Fang et al. [10] observe that the gradient norm on real and fake data diverges when D starts to overfit.

3 A Roadmap to a New Baseline — R3GAN

The well-behaved RpGAN + R_1 + R_2 loss alleviates GAN optimization problems, and lets us proceed to build a minimalist baseline—R3GAN—with recent network backbone advances in mind [48, 97]. Rather than simply state the new approach, we will draw out a roadmap from the StyleGAN2 baseline [30]. This model (Config A; identical to [30]) consists of a VGG-like [73] backbone for G , a ResNet D , a few techniques that facilitate style-based generation, and many tricks that serve as patches to the weak backbone. Then, we remove all non-essential features of StyleGAN2 (Config B), apply our loss function (Config C), and gradually modernize the network backbone (Config D-E).

²Varying γ from 0.1 to 100 does not stabilize training.

³These numbers are from Karras et al. [28], Table 4. “857” corresponds to a low-capacity version of a progressive GAN and “881” adds the minibatch standard deviation trick. Further comparisons via loss curves are difficult since progressive GAN is a substantially different model than the small ResNet we use for this experiment.

We evaluate each configuration on FFHQ 256×256 [29]. Network capacity is kept roughly the same for all configurations—both G and D have about 25 M trainable parameters. Each configuration is trained until D sees 5 M real images. We inherit training hyperparameters (*e.g.*, optimizer settings, batch size, EMA decay length) from Config A unless otherwise specified. We tune the training hyperparameters for our final model and show the converged result in Sec. 4.

Minimum baseline (Config B). We strip away all StyleGAN2 features, retaining only the raw network backbone and basic image generation capability. The features fall into three categories:

- Style-based generation: mapping network [29], style injection [29], weight modulation/demodulation [31], noise injection [29].
- Image manipulation enhancements: mixing regularization [29], path length regularization [31].
- Tricks: z normalization [28], mini-batch stddev [28], equalized learning rate [28], lazy regularization [31].

Following [69, 70], we reduce the dimension of z to 64. The absence of equalized learning rate necessitates a lower learning rate, reduced from 2.5×10^{-3} to 5×10^{-5} . Despite a higher FID of 12.46 than Config-A, this simplified baseline produces reasonable sample quality and stable training. We compare this with DCGAN [60], an early attempt at image generation. Key differences include:

- Convergent training objective with R_1 regularization.
- Smaller learning rate, avoiding momentum optimizer (Adam $\beta_1 = 0$).
- No normalization layer in G or D .
- Proper resampling via bilinear interpolation instead of strided (transposed) convolution.
- Leaky ReLU in both G and D , no tanh in the output layer of G .
- 4×4 constant input for G , output skips for G , ResNet D .

Experimental findings from StyleGAN. Violating **a)**, **b)**, or **c)** often leads to training failures. Gidel *et al.* [11] show that *negative* momentum can improve GAN training dynamics. Since optimal negative momentum is another challenging hyperparameter, we do not use any momentum to avoid worsening GAN training dynamics. Studies suggest normalization layers harm generative models [31, 34]. Batch normalization [21] often cripples training due to dependencies across multiple samples, and is incompatible with R_1 , R_2 , or RpGAN that assume independent handling of each sample. Weaker data-independent normalizations [31, 34] might help; we leave this for future work. Early GANs may succeed despite violating **a)** and **c)**, possibly constituting a full-rank solution [52] to Eq. 1.

Violations of **d)** or **e)** do not significantly impair training stability but negatively affect sample quality. Improper transposed convolution can cause checkerboard artifacts, unresolved even with subpixel convolution [72] or carefully tuned transposed convolution unless a low-pass filter is applied. Interpolation methods avoid this issue, varying from nearest neighbor [28] to Kaiser filters [32]. We use bilinear interpolation for simplicity. For activation functions, smooth approximations of (leaky) ReLU, such as Swish [61], GELU [18], and SMU [2], worsen FID. PReLU [15] marginally improves FID but increases VRAM usage, so we use leaky ReLU.

All subsequent configurations adhere to **a)** through **e)**. Violation of **f)** is acceptable as it pertains to the network backbone of StyleGAN2 [31], modernized in Config D and E.

Well-behaved loss function (Config C). We use the loss function proposed in Section 2 and this reduces FID to 11.65. We hypothesize that the network backbone in Config B is the limiting factor.

General network modernization (Config D). First, we apply the 1-3-1 bottleneck ResNet architecture [16, 17] to both G and D . This is the direct ancestor of all modern vision backbones [48, 97].

	Configuration	FID↓	G #params	D #params
A	StyleGAN2	7.516	24.767M	24.001M
B	Stripped StyleGAN2 - z normalization - Minibatch stddev - Equalized learning rate - Mapping network - Style injection - Weight mod / demod - Noise injection - Mixing regularization - Path length regularization - Lazy regularization	12.46	18.890M	23.996M
C	Well-behaved Loss + RpGAN loss + R_2 gradient penalty	11.77 11.65	18.890M	23.996M
D	ConvNeXt-ify pt. 1 + ResNet-ify G & D - Output skips	10.17 9.950	23.400M 23.378M	23.282M
E	ConvNeXt-ify pt. 2 + ResNeXt-ify G & D + Inverted bottleneck	7.507 7.045	23.188M 23.058M	23.091M 23.010M

Table 2: Effect of our simplification and modernization efforts evaluated on FFHQ-256.

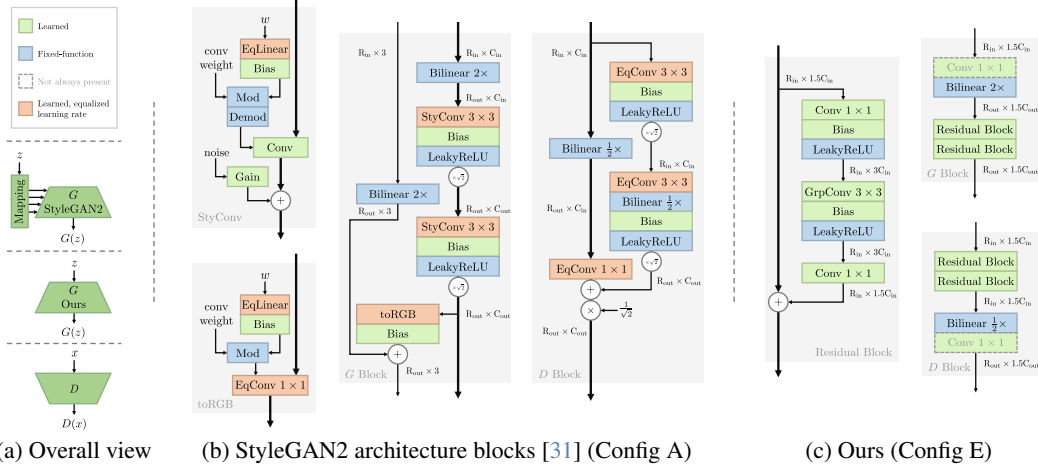


Figure 2: **Architecture comparison.** For image generation, G and D are often both deep ConvNets with either partially or fully symmetric architectures. **(a)** StyleGAN2 [31] G uses a network to map noise vector z to an intermediate style space \mathcal{W} . We use a traditional generator as style mapping is not necessary for a minimal working model. **(b)** StyleGAN2’s building blocks have intricate layers but are themselves simple, with a ConvNet architecture from 2015 [38, 73, 16]. ResNet’s identity mapping principle is also violated in the discriminator. **(c)** We remove tricks and modernize the architecture. Our design has clean layers with a more powerful ConvNet architecture.

We also incorporate principles discovered in Config B and various modernization efforts from ConvNeXt [48]. We categorize the roadmap of ConvNeXt as follows:

- i. Consistently beneficial: i.1) increased width with depthwise convolution, i.2) inverted bottleneck, i.3) fewer activation functions, and i.4) separate resampling layers.
- ii. Negligible performance gain: ii.1) large kernel depthwise conv. with fewer channels, ii.2) swap ReLU with GELU, ii.3) fewer normalization layers, and ii.4) swap batch norm. with layer norm.
- iii. Irrelevant to our setting: iii.1) improved training recipe, iii.2) stage ratio, and iii.3) ‘patchify’ stem.

We aim to apply i) to our model, specifically i.3 and i.4 for the classic ResNet, while reserving i.1 and i.2 for Config E. Many aspects of ii) were introduced merely to mimic vision transformers [47, 9] without yielding significant improvements [48]. ii.3 and ii.4 are inapplicable due to our avoidance of normalization layers following principle c). ii.2 contradicts our finding that GELU deteriorates GAN performance, thus we use leaky ReLU per principle e). Liu *et al.* emphasize large conv. kernels (ii.1) [48], but this results in slightly worse performance compared to wider 3×3 conv. layers, so we do not adopt this ConvNeXt design choice.

Neural network architecture details. Given i.3, i.4, and principles c), d), and e), we can replace the StyleGAN2 backbone with a modernized ResNet. We use a fully symmetric design for G and D with 25 M parameters each, comparable to Config-A. The architecture is minimalist: each resolution stage has one transition layer and two residual blocks. The transition layer consists of bilinear resampling and an optional 1×1 conv. for changing spatial size and feature map channels. The residual block includes five operations: $\text{Conv}1 \times 1 \rightarrow \text{Leaky ReLU} \rightarrow \text{Conv}3 \times 3 \rightarrow \text{Leaky ReLU} \rightarrow \text{Conv}1 \times 1$, with the final $\text{Conv}1 \times 1$ having no bias term. For the 4×4 resolution stage, the transition layer is replaced by a basis layer for G and a classifier head for D . The basis layer, similar to StyleGAN [29, 31], uses 4×4 learnable feature maps modulated by z via a linear layer. The classifier head uses a global 4×4 depthwise conv. to remove spatial extent, followed by a linear layer to produce D ’s output. We maintain the width ratio for each resolution stage as in Config A, making the stem width $3 \times$ as wide due to the efficient 1×1 conv. The 3×3 conv. in the residual block has a compression ratio of 4, following [16, 17], making the bottleneck width $0.75 \times$ as wide as Config A.

To avoid variance explosion due to the lack of normalization, we employ fix-up initialization [99]: We zero-initialize the last convolutional layer in each residual block and scale down the initialization of the other two convolutional layers in the block by $L^{-0.25}$, where L is the number of residual blocks. We avoid other fix-up tricks, such as excessive bias terms and a learnable multiplier.

Bottleneck modernization (Config E). Now that we have settled on the overall architecture, we investigate how the residual block can be modernized, specifically i.1) and i.2). First, we explore i.1 and replace the 3×3 convolution in the residual block with a grouped convolution. We set the group size to 16 rather than 1 (*i.e.* depthwise convolution as in ConvNeXt) as depthwise convolution is highly inefficient on GPUs and is not much faster than using a larger group size. With grouped convolution, we can reduce the bottleneck compression ratio to two given the same model size. This increases the width of the bottleneck to $1.5\times$ as wide as Config A. Finally, we notice that the compute cost of grouped convolution is negligible compared to 1×1 convolution, and so we seek to enhance the capacity of grouped convolution. We apply i.2), which inverts the bottleneck width and the stem width, and which doubles the width of grouped convolutions without any increase in model size. Figure 2 depicts our final design, which reflects modern CNN architectures.

4 Experiments Details

4.1 Roadmap Insights on FFHQ-256 [29]

As per Table 2, Config A (vanilla StyleGAN2) achieves an FID of 7.52 using the official implementation on FFHQ-256. Config B with all tricks removed achieves an FID of 12.46—performance drops as expected. Config C, with a well-behaved loss, achieves an FID of 11.65. But, now training is sufficiently stable to improve the architecture.

Config D, which improves G and D based on the classic ResNet and ConvNeXt findings, achieves an FID of 9.95. The output skips of the StyleGAN2 generator are no longer useful given our new architecture; including them produces a worse FID of 10.17. Karras *et al.* find that the benefit of output skips is mostly related to gradient magnitude dynamics [32], and this has been addressed by our ResNet architecture. For StyleGAN2, Karras *et al.* conclude that a ResNet architecture is harmful to G [31], but this is not true in our case as their ResNet implementation is considerably different from ours: 1) Karras *et al.* use one 3-3 residual block for each resolution stage, while we have a separate transition layer and two 1-3-1 residual blocks; 2) i.3) and i.4) are violated as they do not have a linear residual block [67] and the transition layer is placed on the skip branch of the residual block rather than the stem; 3) the essential principle of ResNet [16]—identity mapping [17]—is violated as Karras *et al.* divide the output of the residual block by $\sqrt{2}$ to avoid variance explosion due to the absence of a proper initialization scheme.

For Config E, we conduct two experiments that ablate i.1 (increased width with depthwise conv.) and i.2 (an inverted bottleneck). We add GroupedConv and reduce the bottleneck compression ratio to two given the same model size. Each bottleneck is now $1.5\times$ the width of Config A, and the FID drops to 7.51, surpassing the performance of StyleGAN2. By inverting the stem and the bottleneck dimensions to enhance the capacity of GroupedConv, our final model achieves an FID of 7.05, exceeding StyleGAN2.

4.2 Mode Recovery — StackedMNIST [53]

We repeat the earlier experiment in 1000-mode convergence on StackedMNIST (unconditional generation), but this time with our updated architecture and with comparisons to SOTA GANs and likelihood-based methods (Tab. 3, Fig. 5). One advantage brought up of likelihood-based models such as diffusion over GANs is that they achieve mode coverage [7]. We find that most GANs struggle to find all modes. But, PresGAN [8], DDGAN [94], and our approach are successful. Further, our method outperforms all other tested GAN models in term of KL divergence.

Model	# modes \uparrow	$D_{KL}\downarrow$
DCGAN [60]	99	3.40
VEEGAN [80]	150	2.95
WGAN-GP [14]	959	0.73
PacGAN [46]	992	0.28
StyleGAN2 [31]	940	0.42
PresGAN [8]	1000	0.12
Adv. DSM [24]	1000	1.49
VAEBM [93]	1000	0.087
DDGAN [94]	1000	0.071
MEG [39]	1000	0.031
Ours—Config E	1000	0.029

Table 3: StackedMNIST 1000-mode coverage.

4.3 FID — FFHQ-256 [29] (Optimized)

We train Config E model until convergence and with optimized hyperparameters and training schedule on FFHQ at 256×256 (unconditional generation) (Tab. 4, Figs. 4 and 6). Please see our supplemental material for training details. Our model outperforms existing StyleGAN methods, plus four more

Model	NFE↓	FID↓
StyleGAN2 [31]	1	3.78
StyleGAN3-T [32]	1	4.81
StyleGAN3-R [32]	1	3.92
LDM [62]	200	4.98
ADM (DDIM) [7, 49]	500	8.41
ADM (DPM-Solver) [7, 49]	500	8.40
Diffusion Autoencoder [59, 49]	500	5.81
Ours—Config E	1	2.75
<i>With ImageNet feature leakage [41]:</i>		
PolyINR* [74]	1	2.72
StyleGAN-XL* [69]	1	2.19
StyleSAN-XL* [82]	1	1.68

Table 4: FFHQ-256. * denotes models that leak ImageNet features.

Model	NFE↓	FID↓
StyleGAN2 [31, 45]	1	3.32
MSG-GAN [27, 45]	1	2.7
Anycost GAN [45]	1	2.52
VE [78, 33]	79	25.95
VP [78, 33]	79	3.39
EDM [33]	79	2.39
Ours—Config E	1	1.95

Table 5: FFHQ-64.

recent diffusion-based methods. On this common dataset experimental setting, many methods (not listed here) use the bCR [101] trick—this has only been shown to improve performance on FFHQ-256 (not even at different resolutions of FFHQ) [101, 98]. We do not use this trick.

4.4 FID — FFHQ-64 [33]

To compare with EDM [33] directly, we evaluate our model on FFHQ at 64×64 resolution. For this, we remove the two highest resolution stages of our 256×256 model, resulting in a generator that is less than half the number of parameters as EDM. Despite this, our model outperforms EDM on this dataset and needs one function evaluation only (Tab. 5).

4.5 FID — CIFAR-10 [37]

We train Config E model until convergence and with optimized hyperparameters and training schedule on CIFAR-10 (conditional generation) (Tab. 6, Fig. 8). Our method outperforms many other GANs by FID even though the model has relatively small capacity. For instance, StyleGAN-XL [69] has 18 M parameters in the generator and 125 M parameters in the discriminator, while our model has a 40 M parameters between the generator and discriminator combined (Fig. 3). Compared to diffusion models like LDM or ADM, GAN inference is significantly cheaper as it requires only one network function evaluation compared to the tens or hundreds of network function evaluations for diffusion models without distillation.

Many state-of-the-art GANs are derived from Projected GAN [68], including StyleGAN-XL [69] and the concurrent work of StyleSAN-XL [82]. These methods use a pre-trained ImageNet classifier in the discriminator. Prior work has shown that a pre-trained ImageNet discriminator can leak ImageNet features into the model [41], causing the model to perform better when evaluating on FID since it relies on a pre-trained ImageNet classifier for the loss. But, this does not improve results in perceptual studies [41]. Our model produces its low FID without any ImageNet pre-training.

Model	NFE↓	FID↓
BigGAN [3]	1	14.73
TransGAN [87]	1	9.26
ViTGAN [42]	1	6.66
DDGAN [94]	4	3.75
Diffusion StyleGAN2 [90]	1	3.19
StyleGAN2 + ADA [30]	1	2.42
StyleGAN3-R + ADA [32, 25]	1	10.83
DDPM [20]	1000	3.21
DDIM [76]	50	4.67
VE [78, 33]	35	3.11
VP [78, 33]	35	2.48
Ours—Config E	1	1.96
<i>With ImageNet feature leakage [41]:</i>		
StyleGAN-XL* [69]	1	1.85

Table 6: CIFAR-10 performance.

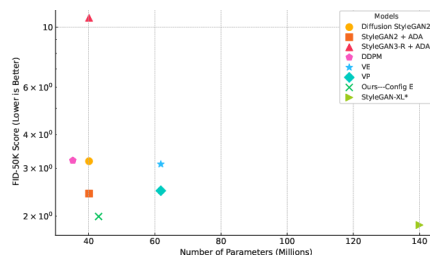


Figure 3: Millions of parameters vs. FID-50K (log scale) on CIFAR-10. Lower is better.

Model	NFE↓	FID↓
DDPM++ [35]	1000	8.42
VDM [36]	1000	7.41
MSGAN [27, 56]	1	12.3
ADM [7]	1000	3.60
DDPM-IP [56]	1000	2.87
Ours—Config E	1	1.27
<i>With ImageNet feature leakage [41]:</i>		
StyleGAN-XL* [69]	1	1.10

Table 7: ImageNet-32.

Model	NFE↓	FID↓
BigGAN-deep [3]	1	4.06
DDPM [20]	250	11.0
DDIM [76]	50	13.7
ADM [7]	§250	2.91
EDM [33]	79	2.23
CT [79]	2	11.1
CD [79]	3	4.32
iCT-deep [77]	2	2.77
DMD [96]	1	2.62
Ours—Config E	1	2.09
<i>With ImageNet feature leakage [41]:</i>		
StyleGAN-XL* [69]	1	1.52

Table 8: ImageNet-64. §deterministic sampling.

4.6 FID — ImageNet-32 [6]

We train Config E model until convergence and with optimized hyperparameters and training schedule on ImageNet-32 (conditional generation). We compare against recent GAN models and recent diffusion models in Table 7. We adjust the number of parameters in the generator of our model to match StyleGAN-XL [69]’s generator (84M parameters). Specifically, we make the model significantly wider to match. Our method achieves comparable FID despite using a 60% smaller discriminator (Tab. 7) and despite not using a pre-trained ImageNet classifier.

4.7 FID — ImageNet-64 [6]

We evaluate our model on ImageNet-64 to test its scalability. We stack another resolution stage on our ImageNet-32 model, resulting in a generator of 104 M parameters. This model is nearly $3\times$ smaller than diffusion-like models [7, 33, 79, 77] that rely on the ADM backbone, which contains about 300 M parameters. Despite the smaller model size and that our model generates samples in one step, it outperforms larger diffusion models with many NFEs on FID (Tab. 8).

4.8 Recall

We evaluate the recall [40] of our model on each dataset to quantify sample diversity. In general, our model achieves a recall that is similar to or marginally worse than the diffusion model counterpart, yet superior to existing GAN models. For CIFAR-10, the recall of our model peaked at 0.57; as a point of comparison, StyleGAN-XL [69] has a worse recall of 0.47 despite its lower FID. For FFHQ, we obtain a recall of 0.53 at 64×64 and 0.49 at 256×256 , whereas StyleGAN2 [31] achieved a recall of 0.43 on FFHQ-256. Our ImageNet-32 model achieved a recall of 0.63; comparable to ADM [7]. Our ImageNet-64 model achieved recall 0.59. While this is slightly worse than ≈ 0.63 that many diffusion models achieve, it is better than BigGAN-deep [3] which achieved a recall of 0.48.

5 Discussion and Limitations

We have shown that a simplification of GANs is possible for image generation tasks, built upon a more stable $R_p\text{GAN}+R_1+R_2$ objective with mathematically-demonstrated convergence properties that still provides diverse output. This stability is what lets us re-engineer a modern network architecture without the tricks of previous methods, producing the R3GAN model with competitive FID on the common datasets of Stacked-MNIST, FFHQ, CIFAR-10, and ImageNet as an empirical demonstration of the mathematical benefits.

The focus of our work is to elucidate the essential components of a minimum GAN for image generation. As such, we prioritize simplicity over functionality—we do not claim to beat the performance of every existing model on every dataset or task; merely to provide a new simple



Figure 4: Qualitative examples of sample generation from our Config E on FFHQ-256.

baseline that converges easily. While this makes our model a possible backbone for future GANs, it also means that it is not suitable to apply our model directly to downstream applications such as image editing or controllable generation, as our model lacks dedicated features for easy image inversion or disentangled image synthesis. For instance, we remove style injection functionality from StyleGAN even though this has a clear use. We also omitted common techniques that have been shown in previous literature to improve FID considerably. Examples include some form of adaptive normalization modulated by the latent code [7, 33, 29, 98, 58, 89, 66], and using multiheaded self attention at lower resolution stages [7, 33, 34]. We aim to explore these techniques in a future study.

Further, our work is limited in its evaluation of the scalability of R3GAN models. While they show promising results on 64×64 ImageNet, we are yet to verify the scalability on higher resolution ImageNet data or large-scale text to image generation tasks [12].

Finally, as a method that can improve the quality of generative models, it would be amiss not to mention that generative models—especially of people—can cause direct harm (e.g., through personalized deep fakes) and societal harm through the spread of disinformation (e.g., fake influencers).

6 Conclusion

This work introduced R3GAN, a new baseline GAN that features increased stability, leverages modern architectures, and does not require ad-hoc tricks that are commonplace in existing GAN models. Central to our approach is a regularized relativistic loss that provably features local convergence and that improves the stability of GAN training. This stable loss enables us to ablate various tricks that were previously necessary in GANs, and incorporate in their place modern deep architectures. The resulting streamlined baseline achieves competitive performance to SOTA models within its parameter size class. We anticipate that our backbone will help to drive future GAN research.

Acknowledgements. The authors thank Xinjie Jayden Yi for contributing to the proof and Yu Cheng for helpful discussion. For compute, the authors thank Databricks Mosaic Research. Yiwen Huang was supported by a Brown University Division of Research Seed Award, and James Tompkin was supported by NSF CAREER 2144956. Volodymyr Kuleshov was supported by NSF CAREER 2145577 and NIH MIRA 1R35GM15124301.

References

- [1] Jimmy Lei Ba, Jamie Ryan Kiros, and Geoffrey E Hinton. Layer normalization. *arXiv preprint arXiv:1607.06450*, 2016.
- [2] Koushik Biswas, Sandeep Kumar, Shilpak Banerjee, and Ashish Kumar Pandey. Smu: smooth activation function for deep networks using smoothing maximum technique. *arXiv preprint arXiv:2111.04682*, 2021.
- [3] Andrew Brock, Jeff Donahue, and Karen Simonyan. Large scale gan training for high fidelity natural image synthesis. *arXiv preprint arXiv:1809.11096*, 2018.
- [4] Andy Brock, Soham De, Samuel L Smith, and Karen Simonyan. High-performance large-scale image recognition without normalization. In *International Conference on Machine Learning*, pp. 1059–1071. PMLR, 2021.
- [5] François Chollet. Xception: Deep learning with depthwise separable convolutions. In *Proceedings of the IEEE conference on computer vision and pattern recognition*, pp. 1251–1258, 2017.
- [6] Patryk Chrabaszcz, Ilya Loshchilov, and Frank Hutter. A downsampled variant of imagenet as an alternative to the cifar datasets. *arXiv preprint arXiv:1707.08819*, 2017.
- [7] Prafulla Dhariwal and Alexander Nichol. Diffusion models beat gans on image synthesis. *Advances in neural information processing systems*, 34:8780–8794, 2021.
- [8] Adji B Dieng, Francisco JR Ruiz, David M Blei, and Michalis K Titsias. Prescribed generative adversarial networks. *arXiv preprint arXiv:1910.04302*, 2019.
- [9] Alexey Dosovitskiy, Lucas Beyer, Alexander Kolesnikov, Dirk Weissenborn, Xiaohua Zhai, Thomas Unterthiner, Mostafa Dehghani, Matthias Minderer, Georg Heigold, Sylvain Gelly, et al. An image is worth 16x16 words: Transformers for image recognition at scale. *arXiv preprint arXiv:2010.11929*, 2020.
- [10] Tiantian Fang, Ruoyu Sun, and Alex Schwing. DigGAN: Discriminator gradient gap regularization for GAN training with limited data. In Alice H. Oh, Alekh Agarwal, Danielle Belgrave, and Kyunghyun Cho (eds.), *Advances in Neural Information Processing Systems*, 2022. URL https://openreview.net/forum?id=azBVn74t_2.
- [11] Gauthier Gidel, Reyhane Askari Hemmat, Mohammad Pezeshki, Rémi Le Priol, Gabriel Huang, Simon Lacoste-Julien, and Ioannis Mitliagkas. Negative momentum for improved game dynamics. In *The 22nd International Conference on Artificial Intelligence and Statistics*, pp. 1802–1811. PMLR, 2019.
- [12] Aaron Gokaslan, A Feder Cooper, Jasmine Collins, Landan Seguin, Austin Jacobson, Mihir Patel, Jonathan Frankle, Cory Stephenson, and Volodymyr Kuleshov. Commoncanvas: Open diffusion models trained on creative-commons images. In *Proceedings of the IEEE/CVF Conference on Computer Vision and Pattern Recognition*, pp. 8250–8260, 2024.
- [13] Ian Goodfellow, Jean Pouget-Abadie, Mehdi Mirza, Bing Xu, David Warde-Farley, Sherjil Ozair, Aaron Courville, and Yoshua Bengio. Generative adversarial networks. *Communications of the ACM*, 63(11): 139–144, 2020.
- [14] Ishaan Gulrajani, Faruk Ahmed, Martin Arjovsky, Vincent Dumoulin, and Aaron C Courville. Improved training of wasserstein gans. *Advances in neural information processing systems*, 30, 2017.
- [15] Kaiming He, Xiangyu Zhang, Shaoqing Ren, and Jian Sun. Delving deep into rectifiers: Surpassing human-level performance on imagenet classification. In *Proceedings of the IEEE international conference on computer vision*, pp. 1026–1034, 2015.
- [16] Kaiming He, Xiangyu Zhang, Shaoqing Ren, and Jian Sun. Deep residual learning for image recognition. In *Proceedings of the IEEE conference on computer vision and pattern recognition*, pp. 770–778, 2016.

- [17] Kaiming He, Xiangyu Zhang, Shaoqing Ren, and Jian Sun. Identity mappings in deep residual networks. In *Computer Vision—ECCV 2016: 14th European Conference, Amsterdam, The Netherlands, October 11–14, 2016, Proceedings, Part IV 14*, pp. 630–645. Springer, 2016.
- [18] Dan Hendrycks and Kevin Gimpel. Gaussian error linear units (gelus). *arXiv preprint arXiv:1606.08415*, 2016.
- [19] Martin Heusel, Hubert Ramsauer, Thomas Unterthiner, Bernhard Nessler, and Sepp Hochreiter. Gans trained by a two time-scale update rule converge to a local nash equilibrium. *Advances in neural information processing systems*, 30, 2017.
- [20] Jonathan Ho, Ajay Jain, and Pieter Abbeel. Denoising diffusion probabilistic models. *Advances in neural information processing systems*, 33:6840–6851, 2020.
- [21] Sergey Ioffe and Christian Szegedy. Batch normalization: Accelerating deep network training by reducing internal covariate shift. In *International conference on machine learning*, pp. 448–456. pmlr, 2015.
- [22] Alexia Jolicoeur-Martineau. The relativistic discriminator: a key element missing from standard gan. *arXiv preprint arXiv:1807.00734*, 2018.
- [23] Alexia Jolicoeur-Martineau and Ioannis Mitliagkas. Gradient penalty from a maximum margin perspective. *arXiv preprint arXiv:1910.06922*, 2019.
- [24] Alexia Jolicoeur-Martineau, Rémi Piché-Taillefer, Rémi Tachet des Combes, and Ioannis Mitliagkas. Adversarial score matching and improved sampling for image generation. *arXiv preprint arXiv:2009.05475*, 2020.
- [25] Minguk Kang, Joonghyuk Shin, and Jaesik Park. Studiogan: a taxonomy and benchmark of gans for image synthesis. *IEEE Transactions on Pattern Analysis and Machine Intelligence*, 2023.
- [26] Minguk Kang, Jun-Yan Zhu, Richard Zhang, Jaesik Park, Eli Shechtman, Sylvain Paris, and Taesung Park. Scaling up gans for text-to-image synthesis. In *Proceedings of the IEEE/CVF Conference on Computer Vision and Pattern Recognition*, pp. 10124–10134, 2023.
- [27] Animesh Karnewar and Oliver Wang. Msg-gan: Multi-scale gradients for generative adversarial networks. In *Proceedings of the IEEE/CVF conference on computer vision and pattern recognition*, pp. 7799–7808, 2020.
- [28] Tero Karras, Timo Aila, Samuli Laine, and Jaakko Lehtinen. Progressive growing of gans for improved quality, stability, and variation. *arXiv preprint arXiv:1710.10196*, 2017.
- [29] Tero Karras, Samuli Laine, and Timo Aila. A style-based generator architecture for generative adversarial networks. In *Proceedings of the IEEE/CVF conference on computer vision and pattern recognition*, pp. 4401–4410, 2019.
- [30] Tero Karras, Miika Aittala, Janne Hellsten, Samuli Laine, Jaakko Lehtinen, and Timo Aila. Training generative adversarial networks with limited data. *Advances in neural information processing systems*, 33:12104–12114, 2020.
- [31] Tero Karras, Samuli Laine, Miika Aittala, Janne Hellsten, Jaakko Lehtinen, and Timo Aila. Analyzing and improving the image quality of stylegan. In *Proceedings of the IEEE/CVF conference on computer vision and pattern recognition*, pp. 8110–8119, 2020.
- [32] Tero Karras, Miika Aittala, Samuli Laine, Erik Härkönen, Janne Hellsten, Jaakko Lehtinen, and Timo Aila. Alias-free generative adversarial networks. *Advances in Neural Information Processing Systems*, 34:852–863, 2021.
- [33] Tero Karras, Miika Aittala, Timo Aila, and Samuli Laine. Elucidating the design space of diffusion-based generative models. *Advances in Neural Information Processing Systems*, 35:26565–26577, 2022.
- [34] Tero Karras, Miika Aittala, Jaakko Lehtinen, Janne Hellsten, Timo Aila, and Samuli Laine. Analyzing and improving the training dynamics of diffusion models. *arXiv preprint arXiv:2312.02696*, 2023.
- [35] Dongjun Kim, Seungjae Shin, Kyungwoo Song, Wanmo Kang, and Il-Chul Moon. Soft truncation: A universal training technique of score-based diffusion model for high precision score estimation. *arXiv preprint arXiv:2106.05527*, 2021.
- [36] Diederik Kingma, Tim Salimans, Ben Poole, and Jonathan Ho. Variational diffusion models. *Advances in neural information processing systems*, 34:21696–21707, 2021.

- [37] Alex Krizhevsky, Geoffrey Hinton, et al. Learning multiple layers of features from tiny images. *Thesis*, 2009.
- [38] Alex Krizhevsky, Ilya Sutskever, and Geoffrey E Hinton. Imagenet classification with deep convolutional neural networks. In F. Pereira, C.J. Burges, L. Bottou, and K.Q. Weinberger (eds.), *Advances in Neural Information Processing Systems*, volume 25. Curran Associates, Inc., 2012. URL https://proceedings.neurips.cc/paper_files/paper/2012/file/c399862d3b9d6b76c8436e924a68c45b-Paper.pdf.
- [39] Rithesh Kumar, Sherjil Ozair, Anirudh Goyal, Aaron Courville, and Yoshua Bengio. Maximum entropy generators for energy-based models. *arXiv preprint arXiv:1901.08508*, 2019.
- [40] Tuomas Kynkäänniemi, Tero Karras, Samuli Laine, Jaakko Lehtinen, and Timo Aila. Improved precision and recall metric for assessing generative models. *Advances in neural information processing systems*, 32, 2019.
- [41] Tuomas Kynkäänniemi, Tero Karras, Miika Aittala, Timo Aila, and Jaakko Lehtinen. The role of imagenet classes in fréchet inception distance. *arXiv preprint arXiv:2203.06026*, 2022.
- [42] Kwonjoon Lee, Huiwen Chang, Lu Jiang, Han Zhang, Zhuowen Tu, and Ce Liu. Vitgan: Training gans with vision transformers. *arXiv preprint arXiv:2107.04589*, 2021.
- [43] Bee Lim, Sanghyun Son, Heewon Kim, Seungjun Nah, and Kyoung Mu Lee. Enhanced deep residual networks for single image super-resolution. In *Proceedings of the IEEE conference on computer vision and pattern recognition workshops*, pp. 136–144, 2017.
- [44] Jae Hyun Lim and Jong Chul Ye. Geometric gan. *arXiv preprint arXiv:1705.02894*, 2017.
- [45] Ji Lin, Richard Zhang, Frieder Ganz, Song Han, and Jun-Yan Zhu. Anycost gans for interactive image synthesis and editing. In *Proceedings of the IEEE/CVF Conference on Computer Vision and Pattern Recognition*, pp. 14986–14996, 2021.
- [46] Zinan Lin, Ashish Khetan, Giulia Fanti, and Sewoong Oh. Pacgan: The power of two samples in generative adversarial networks. *Advances in neural information processing systems*, 31, 2018.
- [47] Ze Liu, Yutong Lin, Yue Cao, Han Hu, Yixuan Wei, Zheng Zhang, Stephen Lin, and Baining Guo. Swin transformer: Hierarchical vision transformer using shifted windows. In *Proceedings of the IEEE/CVF international conference on computer vision*, pp. 10012–10022, 2021.
- [48] Zhuang Liu, Hanzi Mao, Chao-Yuan Wu, Christoph Feichtenhofer, Trevor Darrell, and Saining Xie. A convnet for the 2020s. In *Proceedings of the IEEE/CVF Conference on Computer Vision and Pattern Recognition*, pp. 11976–11986, 2022.
- [49] Hui Lu, Ronald Poppe, et al. Compensation sampling for improved convergence in diffusion models. *arXiv preprint arXiv:2312.06285*, 2023.
- [50] Xudong Mao, Qing Li, Haoran Xie, Raymond YK Lau, Zhen Wang, and Stephen Paul Smolley. Least squares generative adversarial networks. In *Proceedings of the IEEE international conference on computer vision*, pp. 2794–2802, 2017.
- [51] Lars Mescheder, Sebastian Nowozin, and Andreas Geiger. The numerics of gans. *Advances in neural information processing systems*, 30, 2017.
- [52] Lars Mescheder, Andreas Geiger, and Sebastian Nowozin. Which training methods for gans do actually converge? In *International conference on machine learning*, pp. 3481–3490. PMLR, 2018.
- [53] Luke Metz, Ben Poole, David Pfau, and Jascha Sohl-Dickstein. Unrolled generative adversarial networks. In *International Conference on Learning Representations*, 2016.
- [54] Takeru Miyato and Masanori Koyama. cgans with projection discriminator. *arXiv preprint arXiv:1802.05637*, 2018.
- [55] Vaishnavh Nagarajan and J Zico Kolter. Gradient descent gan optimization is locally stable. *Advances in neural information processing systems*, 30, 2017.
- [56] Mang Ning, Enver Sangineto, Angelo Porrello, Simone Calderara, and Rita Cucchiara. Input perturbation reduces exposure bias in diffusion models. *arXiv preprint arXiv:2301.11706*, 2023.
- [57] Sebastian Nowozin, Botond Cseke, and Ryota Tomioka. f-gan: Training generative neural samplers using variational divergence minimization. *Advances in neural information processing systems*, 29, 2016.

- [58] William Peebles and Saining Xie. Scalable diffusion models with transformers. In *Proceedings of the IEEE/CVF International Conference on Computer Vision*, pp. 4195–4205, 2023.
- [59] Konpat Preechakul, Nattanat Chatthee, Suttisak Wizadwongsa, and Supasorn Suwajanakorn. Diffusion autoencoders: Toward a meaningful and decodable representation. In *Proceedings of the IEEE/CVF Conference on Computer Vision and Pattern Recognition (CVPR)*, pp. 10619–10629, June 2022.
- [60] Alec Radford, Luke Metz, and Soumith Chintala. Unsupervised representation learning with deep convolutional generative adversarial networks. *arXiv preprint arXiv:1511.06434*, 2015.
- [61] Prajit Ramachandran, Barret Zoph, and Quoc V Le. Searching for activation functions. *arXiv preprint arXiv:1710.05941*, 2017.
- [62] Robin Rombach, Andreas Blattmann, Dominik Lorenz, Patrick Esser, and Björn Ommer. High-resolution image synthesis with latent diffusion models. In *Proceedings of the IEEE/CVF conference on computer vision and pattern recognition*, pp. 10684–10695, 2022.
- [63] Olaf Ronneberger, Philipp Fischer, and Thomas Brox. U-net: Convolutional networks for biomedical image segmentation. In *Medical image computing and computer-assisted intervention–MICCAI 2015: 18th international conference, Munich, Germany, October 5-9, 2015, proceedings, part III 18*, pp. 234–241. Springer, 2015.
- [64] Kevin Roth, Aurelien Lucchi, Sebastian Nowozin, and Thomas Hofmann. Stabilizing training of generative adversarial networks through regularization. *Advances in neural information processing systems*, 30, 2017.
- [65] Seyedmorteza Sadat, Jakob Buhmann, Derek Bradley, Otmar Hilliges, and Romann M Weber. Litevae: Lightweight and efficient variational autoencoders for latent diffusion models. *arXiv preprint arXiv:2405.14477*, 2024.
- [66] Subham Sekhar Sahoo, Aaron Gokaslan, Chris De Sa, and Volodymyr Kuleshov. Diffusion models with learned adaptive noise. *arXiv preprint arXiv:2312.13236*, 2023.
- [67] Mark Sandler, Andrew Howard, Menglong Zhu, Andrey Zhmoginov, and Liang-Chieh Chen. Mobilenetv2: Inverted residuals and linear bottlenecks. In *Proceedings of the IEEE conference on computer vision and pattern recognition*, pp. 4510–4520, 2018.
- [68] Axel Sauer, Kashyap Chitta, Jens Müller, and Andreas Geiger. Projected gans converge faster. *Advances in Neural Information Processing Systems*, 34:17480–17492, 2021.
- [69] Axel Sauer, Katja Schwarz, and Andreas Geiger. StyleGAN-XL: Scaling stylegan to large diverse datasets. In *ACM SIGGRAPH 2022 conference proceedings*, pp. 1–10, 2022.
- [70] Axel Sauer, Tero Karras, Samuli Laine, Andreas Geiger, and Timo Aila. Stylegan-t: Unlocking the power of gans for fast large-scale text-to-image synthesis. In *International conference on machine learning*, pp. 30105–30118. PMLR, 2023.
- [71] Wenzhe Shi, Jose Caballero, Ferenc Huszár, Johannes Totz, Andrew P Aitken, Rob Bishop, Daniel Rueckert, and Zehan Wang. Real-time single image and video super-resolution using an efficient sub-pixel convolutional neural network. In *Proceedings of the IEEE conference on computer vision and pattern recognition*, pp. 1874–1883, 2016.
- [72] Wenzhe Shi, Jose Caballero, Ferenc Huszár, Johannes Totz, Andrew P Aitken, Rob Bishop, Daniel Rueckert, and Zehan Wang. Real-time single image and video super-resolution using an efficient sub-pixel convolutional neural network. In *Proceedings of the IEEE conference on computer vision and pattern recognition*, pp. 1874–1883, 2016.
- [73] Karen Simonyan and Andrew Zisserman. Very deep convolutional networks for large-scale image recognition. *arXiv preprint arXiv:1409.1556*, 2014.
- [74] Rajhans Singh, Ankita Shukla, and Pavan Turaga. Polynomial implicit neural representations for large diverse datasets. In *Proceedings of the IEEE/CVF Conference on Computer Vision and Pattern Recognition*, pp. 2041–2051, 2023.
- [75] Casper Kaae Sønderby, Jose Caballero, Lucas Theis, Wenzhe Shi, and Ferenc Huszár. Amortised map inference for image super-resolution. *arXiv preprint arXiv:1610.04490*, 2016.
- [76] Jiaming Song, Chenlin Meng, and Stefano Ermon. Denoising diffusion implicit models. In *International Conference on Learning Representations*, 2021.

- [77] Yang Song and Prafulla Dhariwal. Improved techniques for training consistency models. In *The Twelfth International Conference on Learning Representations*, 2024.
- [78] Yang Song, Jascha Sohl-Dickstein, Diederik P Kingma, Abhishek Kumar, Stefano Ermon, and Ben Poole. Score-based generative modeling through stochastic differential equations. *arXiv preprint arXiv:2011.13456*, 2020.
- [79] Yang Song, Prafulla Dhariwal, Mark Chen, and Ilya Sutskever. Consistency models. In *International Conference on Machine Learning*, pp. 32211–32252. PMLR, 2023.
- [80] Akash Srivastava, Lazar Valkov, Chris Russell, Michael U Gutmann, and Charles Sutton. Veegan: Reducing mode collapse in gans using implicit variational learning. *Advances in neural information processing systems*, 30, 2017.
- [81] Ruoyu Sun, Tiantian Fang, and Alexander Schwing. Towards a better global loss landscape of gans. *Advances in Neural Information Processing Systems*, 33:10186–10198, 2020.
- [82] Yuhta Takida, Masaaki Imaizumi, Takashi Shibuya, Chieh-Hsin Lai, Toshimitsu Uesaka, Naoki Murata, and Yuki Mitsufuji. SAN: Inducing metrizable of GAN with discriminative normalized linear layer. In *The Twelfth International Conference on Learning Representations*, 2024. URL <https://openreview.net/forum?id=eiF7TU1E8E>.
- [83] Song Tao and Jia Wang. Alleviation of gradient exploding in gans: Fake can be real. In *Proceedings of the IEEE/CVF conference on computer vision and pattern recognition*, pp. 1191–1200, 2020.
- [84] Hoang Thanh-Tung, Truyen Tran, and Svetha Venkatesh. Improving generalization and stability of generative adversarial networks. In *International Conference on Learning Representations*, 2019. URL <https://openreview.net/forum?id=ByxPYjC5KQ>.
- [85] Dmitry Ulyanov, Andrea Vedaldi, and Victor Lempitsky. Instance normalization: The missing ingredient for fast stylization. *arXiv preprint arXiv:1607.08022*, 2016.
- [86] Arash Vahdat, Karsten Kreis, and Jan Kautz. Score-based generative modeling in latent space. *Advances in neural information processing systems*, 34:11287–11302, 2021.
- [87] Ashish Vaswani, Noam Shazeer, Niki Parmar, Jakob Uszkoreit, Llion Jones, Aidan N Gomez, Łukasz Kaiser, and Illia Polosukhin. Attention is all you need. *Advances in neural information processing systems*, 30, 2017.
- [88] Xintao Wang, Ke Yu, Shixiang Wu, Jinjin Gu, Yihao Liu, Chao Dong, Yu Qiao, and Chen Change Loy. Esrgan: Enhanced super-resolution generative adversarial networks. In *Proceedings of the European conference on computer vision (ECCV) workshops*, pp. 0–0, 2018.
- [89] Yingheng Wang, Yair Schiff, Aaron Gokaslan, Weishen Pan, Fei Wang, Christopher De Sa, and Volodymyr Kuleshov. Infodiffusion: Representation learning using information maximizing diffusion models. In *International Conference on Machine Learning*, pp. 36336–36354. PMLR, 2023.
- [90] Zhendong Wang, Huangjie Zheng, Pengcheng He, Weizhu Chen, and Mingyuan Zhou. Diffusion-gan: Training gans with diffusion. In *The Eleventh International Conference on Learning Representations*, 2023.
- [91] Yuxin Wu and Kaiming He. Group normalization. In *Proceedings of the European conference on computer vision (ECCV)*, pp. 3–19, 2018.
- [92] Yuxin Wu and Kaiming He. Group normalization. In *Proceedings of the European conference on computer vision (ECCV)*, pp. 3–19, 2018.
- [93] Zhisheng Xiao, Karsten Kreis, Jan Kautz, and Arash Vahdat. Vaebm: A symbiosis between variational autoencoders and energy-based models. *arXiv preprint arXiv:2010.00654*, 2020.
- [94] Zhisheng Xiao, Karsten Kreis, and Arash Vahdat. Tackling the generative learning trilemma with denoising diffusion gans. *arXiv preprint arXiv:2112.07804*, 2021.
- [95] Saining Xie, Ross Girshick, Piotr Dollár, Zhuowen Tu, and Kaiming He. Aggregated residual transformations for deep neural networks. In *Proceedings of the IEEE conference on computer vision and pattern recognition*, pp. 1492–1500, 2017.
- [96] Tianwei Yin, Michaël Gharbi, Richard Zhang, Eli Shechtman, Fredo Durand, William T Freeman, and Taesung Park. One-step diffusion with distribution matching distillation. In *Proceedings of the IEEE/CVF Conference on Computer Vision and Pattern Recognition*, pp. 6613–6623, 2024.

- [97] Weihao Yu, Mi Luo, Pan Zhou, Chenyang Si, Yichen Zhou, Xinchao Wang, Jiashi Feng, and Shuicheng Yan. Metaformer is actually what you need for vision. In *Proceedings of the IEEE/CVF conference on computer vision and pattern recognition*, pp. 10819–10829, 2022.
- [98] Bowen Zhang, Shuyang Gu, Bo Zhang, Jianmin Bao, Dong Chen, Fang Wen, Yong Wang, and Baining Guo. Styleswin: Transformer-based gan for high-resolution image generation. In *Proceedings of the IEEE/CVF conference on computer vision and pattern recognition*, pp. 11304–11314, 2022.
- [99] Hongyi Zhang, Yann N Dauphin, and Tengyu Ma. Fixup initialization: Residual learning without normalization. *arXiv preprint arXiv:1901.09321*, 2019.
- [100] Richard Zhang. Making convolutional networks shift-invariant again. In *International conference on machine learning*, pp. 7324–7334. PMLR, 2019.
- [101] Zhengli Zhao, Sameer Singh, Honglak Lee, Zizhao Zhang, Augustus Odena, and Han Zhang. Improved consistency regularization for gans. In *Proceedings of the AAAI conference on artificial intelligence*, volume 35, pp. 11033–11041, 2021.

Appendices

A Local convergence

Following [52], GAN training can be formulated as a dynamical system where the update operator is given by $F_h(\theta, \psi) = (\theta, \psi) + hv(\theta, \psi)$. h is the learning rate and v denotes the gradient vector field:

$$v(\theta, \psi) = \begin{pmatrix} -\nabla_{\theta} \mathcal{L}(\theta, \psi) \\ \nabla_{\psi} \mathcal{L}(\theta, \psi) \end{pmatrix} \quad (4)$$

Mescheder et al. [51] showed that local convergence near (θ^*, ψ^*) can be analyzed by examining the spectrum of the Jacobian \mathbf{J}_{F_h} at the equilibrium: if the Jacobian has eigenvalues with absolute value bigger than 1, then training does not converge. On the other hand, if all eigenvalues have absolute value smaller than 1, then training will converge to (θ^*, ψ^*) at a linear rate. If all eigenvalues have absolute value equal to 1, the convergence behavior is undetermined.

Given some calculations [52], we can show that the eigenvalues of the Jacobian of the update operator $\lambda_{\mathbf{J}_{F_h}}$ can be determined by $\lambda_{\mathbf{J}_v}$:

$$\lambda_{\mathbf{J}_{F_h}} = 1 + h\lambda_{\mathbf{J}_v} . \quad (5)$$

That is, given small enough h [52], the training dynamics can instead be examined using $\lambda_{\mathbf{J}_v}$, *i.e.*, the eigenvalues of the Jacobian of the gradient vector field. If all $\lambda_{\mathbf{J}_v}$ have a negative real part, the training will locally converge to (θ^*, ψ^*) at a linear rate. On the other hand, if some $\lambda_{\mathbf{J}_v}$ have a positive real part, the training is not convergent. If all $\lambda_{\mathbf{J}_v}$ have a zero real part, the convergence behavior is inconclusive.

B DiracRpGAN: A demonstration of non-convergence

Summary. To obtain DiracRpGAN, we apply Eq. 2 to the DiracGAN [52] problem setting. After simplification, DiracRpGAN and DiracGAN are different only by a constant. They have the same gradient vector field, therefore all proofs are identical to Mescheder *et al.* [52].

Definition B.1. *The DiracRpGAN consists of a (univariate) generator distribution $p_{\theta} = \delta_{\theta}$ and a linear discriminator $D_{\psi}(x) = \psi \cdot x$. The true data distribution $p_{\mathcal{D}}$ is given by a Dirac distribution concentrated at 0.*

In this setup, the RpGAN training objective is given by:

$$\mathcal{L}(\theta, \psi) = f(\psi\theta) . \quad (6)$$

We can now show analytically that DiracRpGAN does not converge without regularization.

Lemma B.2. *The unique equilibrium point of the training objective in Eq. 6 is given by $\theta = \psi = 0$. Moreover, the Jacobian of the gradient vector field at the equilibrium point has the two eigenvalues $\pm f'(0)i$ which are both on the imaginary axis.*

The gradient vector field v of Eq. 6 is given by:

$$v(\theta, \psi) = \begin{pmatrix} -\nabla_{\theta} \mathcal{L}(\theta, \psi) \\ \nabla_{\psi} \mathcal{L}(\theta, \psi) \end{pmatrix} = \begin{pmatrix} -\psi f'(\psi\theta) \\ \theta f'(\psi\theta) \end{pmatrix} \quad (7)$$

and the Jacobian of v :

$$\mathbf{J}_v = \begin{pmatrix} -\psi^2 f''(\psi\theta) & -f'(\psi\theta) - \psi\theta f''(\psi\theta) \\ f'(\psi\theta) + \psi\theta f''(\psi\theta) & \theta^2 f''(\psi\theta) \end{pmatrix} \quad (8)$$

Evaluating \mathbf{J}_v at the equilibrium point $\theta = \psi = 0$ gives us:

$$\mathbf{J}_v \Big|_{(0,0)} = \begin{pmatrix} 0 & -f'(0) \\ f'(0) & 0 \end{pmatrix} \quad (9)$$

Therefore, the eigenvalues of \mathbf{J}_v are $\lambda_{1/2} = \pm f'(0)i$, both of which have a real part of 0. Thus, the convergence of DiracRpGAN is inconclusive and further analysis is required.

Lemma B.3. *The integral curves of the gradient vector field $v(\theta, \psi)$ do not converge to the equilibrium point. More specifically, every integral curve $(\theta(t), \psi(t))$ of the gradient vector field $v(\theta, \psi)$ satisfies $\theta(t)^2 + \psi(t)^2 = \text{const}$ for all $t \in [0, \infty)$.*

Let $R(\theta, \psi) = \frac{1}{2}(\theta^2 + \psi^2)$, then:

$$\begin{aligned} \frac{d}{dt}R(\theta(t), \psi(t)) &= -\theta(t)\psi(t)f'(\theta(t)\psi(t)) + \psi(t)\theta(t)f'(\theta(t)\psi(t)) \\ &= 0. \end{aligned} \tag{10}$$

We see that the distance between (θ, ψ) and the equilibrium point $(0, 0)$ stays constant. Therefore, training runs in circles and never converges.

Next, we investigate the convergence behavior of DiracRpGAN with regularization. For DiracRpGAN, both R_1 and R_2 can be reduced to the following form:

$$R(\psi) = \frac{\gamma}{2}\psi^2 \tag{11}$$

Lemma B.4. *The eigenvalues of the Jacobian of the gradient vector field for the gradient-regularized DiracRpGAN at the equilibrium point are given by*

$$\lambda_{1/2} = -\frac{\gamma}{2} \pm \sqrt{\frac{\gamma^2}{4} - f'(0)} \tag{12}$$

In particular, for $\gamma > 0$ all eigenvalues have a negative real part. Hence, gradient descent is locally convergent for small enough learning rates.

With regularization, the gradient vector field becomes

$$\tilde{v}(\theta, \psi) = \begin{pmatrix} -\psi f'(\psi\theta) \\ \theta f'(\psi\theta) - \gamma\psi \end{pmatrix} \tag{13}$$

the Jacobian of \tilde{v} is then given by

$$\mathbf{J}_{\tilde{v}} = \begin{pmatrix} -\psi^2 f''(\psi\theta) & -f'(\psi\theta) - \psi\theta f''(\psi\theta) \\ f'(\psi\theta) + \psi\theta f''(\psi\theta) & \theta^2 f''(\psi\theta) - \gamma \end{pmatrix} \tag{14}$$

evaluating the Jacobian at $\theta = \psi = 0$ yields

$$\mathbf{J}_{\tilde{v}} \Big|_{(0,0)} = \begin{pmatrix} 0 & -f'(0) \\ f'(0) & -\gamma \end{pmatrix} \tag{15}$$

given some calculations, we arrive at Eq.12.

C General Convergence Results

Summary. The proofs are largely the same as Mescheder *et al.* [52]. We use the same proving techniques, and only slightly modify the assumptions and proof details to adapt Mescheder *et al.*'s effort to RpGAN. Like in [52], our proofs do not rely on unrealistic assumptions such as $\text{supp } p_{\mathcal{D}} = \text{supp } p_{\theta}$.

C.1 Assumptions

We closely follow [52] but modify the assumptions wherever necessary to tailor the proofs for RpGAN. Like in [52], we also consider the realizable case where there exists θ such that G_{θ} produces the true data distribution.

Assumption I. *We have $p_{\theta^*} = p_{\mathcal{D}}$, and $D_{\psi^*} = C$ in some local neighborhood of $\text{supp } p_{\mathcal{D}}$, where C is some arbitrary constant.*

Since RpGAN is defined on critic difference rather than raw logits, we no longer require D_{ψ^*} to produce 0 on $\text{supp } p_{\mathcal{D}}$, instead any constant C would suffice.

Assumption II. We have $f'(0) \neq 0$ and $f''(0) < 0$.

This assumption is the same as in [52]. The choice $f(t) = -\log(1 + e^{-t})$ adopted in the main text satisfies this assumption.

As discussed in [52], there generally is not a single equilibrium point (θ^*, ψ^*) , but a submanifold of equivalent equilibria corresponding to different parameterizations of the same function. It is therefore necessary to represent the equilibrium as *reparameterization manifolds* \mathcal{M}_G and \mathcal{M}_D . We modify the reparameterization h as follows:

$$h(\psi) = \mathbb{E}_{\substack{x \sim p_{\mathcal{D}} \\ y \sim \tilde{p}_{\mathcal{D}}}} \left[|D_{\psi}(x) - D_{\psi}(y)|^2 + \|\nabla_x D_{\psi}(x)\|^2 \right] \quad (16)$$

to account for the fact that D_{ψ^*} is now allowed to have any constant value on $\text{supp } p_{\mathcal{D}}$. The *reparameterization manifolds* are then given by:

$$\mathcal{M}_G = \{\theta \mid p_{\theta} = p_{\mathcal{D}}\} \quad (17)$$

$$\mathcal{M}_D = \{\psi \mid h(\psi) = 0\} \quad (18)$$

We assume the same regularity properties as in [52] for \mathcal{M}_G and \mathcal{M}_D near the equilibrium. To state these assumptions, we need:

$$g(\theta) = \mathbb{E}_{x \sim p_{\theta}} [\nabla_{\psi} D_{\psi} |_{\psi=\psi^*}] \quad (19)$$

which leads to:

Assumption III. There are ϵ -balls $B_{\epsilon}(\theta^*)$ and $B_{\epsilon}(\psi^*)$ around θ^* and ψ^* so that $\mathcal{M}_G \cap B_{\epsilon}(\theta^*)$ and $\mathcal{M}_D \cap B_{\epsilon}(\psi^*)$ define C^1 -manifolds. Moreover, the following holds:

- (i) if $v \in \mathbb{R}^n$ is not in $\mathcal{T}_{\psi^*} \mathcal{M}_D$, then $\partial_v^2 h(\psi^*) \neq 0$.
- (ii) if $w \in \mathbb{R}^m$ is not in $\mathcal{T}_{\theta^*} \mathcal{M}_G$, then $\partial_w g(\theta^*) \neq 0$.

These two conditions have exactly the same meanings as in [52]: the first condition indicates the geometry of \mathcal{M}_D can be locally described by the second derivative of h . The second condition implies that D is strong enough that it can detect any deviation from the equilibrium generator distribution. This is the only assumption we have about the expressiveness of D .

C.2 Convergence

We can now show the general convergence result for gradient penalized RpGAN, consider the gradient vector field with either R_1 or R_2 regularization:

$$\tilde{v}_i(\theta, \psi) = \begin{pmatrix} -\nabla_{\theta} \mathcal{L}(\theta, \psi) \\ \nabla_{\psi} \mathcal{L}(\theta, \psi) - \nabla_{\psi} R_i(\theta, \psi) \end{pmatrix} \quad (20)$$

note that the convergence result can also be trivially extended to the case where both R_1 and R_2 are applied. We omit the proof for this case as it is redundant once the convergence with either regularization is proven.

Theorem. Assume Assumption I, II and III hold for (θ^*, ψ^*) . For small enough learning rates, gradient descent for \tilde{v}_1 and \tilde{v}_2 are both convergent to $\mathcal{M}_G \times \mathcal{M}_D$ in a neighborhood of (θ^*, ψ^*) . Moreover, the rate of convergence is at least linear.

We extend the convergence proof by Mescheder *et al.* [52] to our setting. We first prove lemmas necessary to our main proof.

Lemma C.2.1. Assume $J \in \mathbb{R}^{(n+m) \times (n+m)}$ is of the following form:

$$J = \begin{pmatrix} 0 & -B^{\top} \\ B & -Q \end{pmatrix} \quad (21)$$

where $Q \in \mathbb{R}^{m \times m}$ is a symmetric positive definite matrix and $B \in \mathbb{R}^{m \times n}$ has full column rank. Then all eigenvalues λ of J satisfy $\Re(\lambda) < 0$.

Proof. See Mescheder *et al.* [52], Theorem A.7.

Lemma C.2.2. *The gradient of $\mathcal{L}(\theta, \psi)$ w.r.t. θ and ψ are given by:*

$$\nabla_{\theta} \mathcal{L}(\theta, \psi) = \mathbb{E}_{\substack{z \sim p_z \\ x \sim p_D}} [f'(D_{\psi}(G_{\theta}(z)) - D_{\psi}(x)) [\nabla_{\theta} G_{\theta}(z)]^{\top} \nabla_x D_{\psi}(G_{\theta}(z))] \quad (22)$$

$$\nabla_{\psi} \mathcal{L}(\theta, \psi) = \mathbb{E}_{\substack{z \sim p_z \\ x \sim p_D}} [f'(D_{\psi}(G_{\theta}(z)) - D_{\psi}(x)) (\nabla_{\psi} D_{\psi}(G_{\theta}(z)) - \nabla_{\psi} D_{\psi}(x))] \quad (23)$$

Proof. This is just the chain rule.

Lemma C.2.3. *Assume that (θ^*, ψ^*) satisfies Assumption I. The Jacobian of the gradient vector field $v(\theta, \psi)$ at (θ^*, ψ^*) is then*

$$\mathbf{J}_v \Big|_{(\theta^*, \psi^*)} = \begin{pmatrix} 0 & -K_{DG}^{\top} \\ K_{DG} & K_{DD} \end{pmatrix} \quad (24)$$

the terms K_{DD} and K_{DG} are given by

$$K_{DD} = f''(0) \mathbb{E}_{\substack{x \sim p_D \\ y \sim p_D}} [(\nabla_{\psi} D_{\psi^*}(x) - \nabla_{\psi} D_{\psi^*}(y)) (\nabla_{\psi} D_{\psi^*}(x) - \nabla_{\psi} D_{\psi^*}(y))^{\top}] \quad (25)$$

$$K_{DG} = f'(0) \nabla_{\theta} \mathbb{E}_{x \sim p_{\theta}} [\nabla_{\psi} D_{\psi^*}(x)] \Big|_{\theta=\theta^*} \quad (26)$$

Proof. Note that

$$\mathbf{J}_v \Big|_{(\theta^*, \psi^*)} = \begin{pmatrix} -\nabla_{\theta}^2 \mathcal{L}(\theta^*, \psi^*) & -\nabla_{\theta, \psi}^2 \mathcal{L}(\theta^*, \psi^*) \\ \nabla_{\theta, \psi}^2 \mathcal{L}(\theta^*, \psi^*) & \nabla_{\psi}^2 \mathcal{L}(\theta^*, \psi^*) \end{pmatrix} \quad (27)$$

By Assumption I, $D_{\psi^*} = C$ in some neighborhood of $\text{supp } p_D$. Therefore we also have $\nabla_x D_{\psi^*} = 0$ and $\nabla_x^2 D_{\psi^*} = 0$ for $x \in \text{supp } p_D$. Using these two conditions, we see that $\nabla_{\theta}^2 \mathcal{L}(\theta^*, \psi^*) = 0$.

To see Eq.25 and Eq.26, simply take the derivatives of Eq.23 and evaluate at (θ^*, ψ^*) .

Lemma C.2.4. *The gradient $\nabla_{\psi} R_i(\theta, \psi)$ of the regularization terms R_i , $i \in \{1, 2\}$, w.r.t. ψ are*

$$\nabla_{\psi} R_1(\theta, \psi) = \gamma \mathbb{E}_{x \sim p_D} [\nabla_{\psi, x} D_{\psi} \nabla_x D_{\psi}] \quad (28)$$

$$\nabla_{\psi} R_2(\theta, \psi) = \gamma \mathbb{E}_{x \sim p_{\theta}} [\nabla_{\psi, x} D_{\psi} \nabla_x D_{\psi}] \quad (29)$$

Proof. See Mescheder *et al.* [52], Lemma D.3.

Lemma C.2.5. *The second derivatives $\nabla_{\psi}^2 R_i(\theta^*, \psi^*)$ of the regularization terms R_i , $i \in \{1, 2\}$, w.r.t. ψ at (θ^*, ψ^*) are both given by*

$$L_{DD} = \gamma \mathbb{E}_{x \sim p_D} [AA^{\top}] \quad (30)$$

where $A = \nabla_{\psi, x} D_{\psi^*}$. Moreover, both regularization terms satisfy $\nabla_{\theta, \psi} R_i(\theta^*, \psi^*) = 0$.

Proof. See Mescheder *et al.* [52], Lemma D.4.

Given Lemma C.2.3, Lemma C.2.5 and Eq.20, we can now show that the Jacobian of the regularized gradient field at the equilibrium point is given by

$$\mathbf{J}_{\bar{v}} \Big|_{(\theta^*, \psi^*)} = \begin{pmatrix} 0 & -K_{DG}^{\top} \\ K_{DG} & M_{DD} \end{pmatrix} \quad (31)$$

where $M_{DD} = K_{DD} - L_{DD}$. To prove our main theorem, we need to examine $\mathbf{J}_{\bar{v}}$ when restricting it to the space orthogonal to $\mathcal{T}_{(\theta^*, \psi^*)} \mathcal{M}_G \times \mathcal{M}_D$.

Lemma C.2.6. *Assume Assumptions II and III hold. If $v \neq 0$ is not in $\mathcal{T}_{\psi^*} \mathcal{M}_D$, then $v^{\top} M_{DD} v < 0$.*

Proof. By Lemma C.2.3 and Lemma C.2.5, we have

$$v^{\top} K_{DD} v = f''(0) \mathbb{E}_{\substack{x \sim p_D \\ y \sim p_D}} [((\nabla_{\psi} D_{\psi^*}(x) - \nabla_{\psi} D_{\psi^*}(y))^{\top} v)^2] \quad (32)$$

$$v^{\top} L_{DD} v = \gamma \mathbb{E}_{x \sim p_D} [\|Av\|^2] \quad (33)$$

By Assumption II, we have $f''(0) < 0$. Therefore $v^{\top} M_{DD} v \leq 0$. Suppose $v^{\top} M_{DD} v = 0$, this implies

$$(\nabla_{\psi} D_{\psi^*}(x) - \nabla_{\psi} D_{\psi^*}(y))^{\top} v = 0 \quad \text{and} \quad Av = 0 \quad (34)$$

for all $(x, y) \in \text{supp } p_{\mathcal{D}} \times \text{supp } p_{\mathcal{D}}$. Recall the definition of $h(\psi)$ from Eq. 16. Using the fact that $D_{\psi^*} = C$ and $\nabla_x D_{\psi^*} = 0$ for $x \in \text{supp } p_{\mathcal{D}}$, we see that the Hessian of $h(\psi)$ at ψ^* is

$$\nabla_{\psi}^2 h(\psi^*) = 2\mathbb{E}_{\substack{x \sim p_{\mathcal{D}} \\ y \sim p_{\mathcal{D}}}} [(\nabla_{\psi} D_{\psi^*}(x) - \nabla_{\psi} D_{\psi^*}(y))(\nabla_{\psi} D_{\psi^*}(x) - \nabla_{\psi} D_{\psi^*}(y))^{\top} + AA^{\top}] \quad (35)$$

The second directional derivative $\partial_v^2 h(\psi)$ is therefore

$$\partial_v^2 h(\psi) = 2\mathbb{E}_{\substack{x \sim p_{\mathcal{D}} \\ y \sim p_{\mathcal{D}}}} \left[|(\nabla_{\psi} D_{\psi^*}(x) - \nabla_{\psi} D_{\psi^*}(y))^{\top} v|^2 + \|Av\|^2 \right] = 0 \quad (36)$$

By Assumption III, this can only hold if $v \in \mathcal{T}_{\psi^*} \mathcal{M}_D$.

Lemma C.2.7. *Assume Assumption III holds. If $w \neq 0$ is not in $\mathcal{T}_{\theta^*} \mathcal{M}_G$, then $K_{DG} w \neq 0$.*

Proof. See Mescheder *et al.* [52], Lemma D.6.

Proof for the main theorem. Given previous lemmas, by choosing local coordinates $\theta(\alpha, \gamma_G)$ and $\psi(\beta, \gamma_D)$ for \mathcal{M}_G and \mathcal{M}_D such that $\theta^* = 0$, $\psi^* = 0$ as well as

$$\mathcal{M}_G = \mathcal{T}_{\theta^*} \mathcal{M}_G = \{0\}^k \times \mathbb{R}^{n-k} \quad (37)$$

$$\mathcal{M}_D = \mathcal{T}_{\psi^*} \mathcal{M}_D = \{0\}^l \times \mathbb{R}^{m-l} \quad (38)$$

our proof is *exactly* the same as Mescheder *et al.* [52], Theorem 4.1.

D Hyperparameters, training configurations, and compute

We implement our models on top of the official StyleGAN3 code base. While the loss function and the models are implemented from scratch, we reuse support code from the existing implementation whenever possible. This includes exponential moving average (EMA) of generator weights [28], non-leaky data augmentation [30], and metric evaluation [32].

Training schedule. To speed up the convergence early in training, we specify a cosine schedule for the following hyperparameters before they reach their target values:

- Learning rate
- γ for R_1 and R_2 regularization
- Adam β_2
- EMA half-life
- Augmentation probability

We call this early training stage the burn-in phase. Burn-in length and schedule for each hyperparameter are listed in Table 9 for each experiment. A schedule for the EMA half-life can already be found in Karras *et al.* [30], albeit they use a linear schedule. A lower initial Adam β_2 is crucial to the initial large learning rate as it allows the optimizer to adapt to the gradient magnitude change much quicker. We use a large initial γ to account for that early in training: p_θ and p_D are far apart and a large γ smooths both distributions more aggressively which makes learning easier. Augmentation is not necessary until D starts to overfit later on; thus, we set the initial augmentation probability to 0.

Dataset augmentation. We apply horizontal flips and non-leaky augmentation [30] to all datasets where augmentation is enabled. Following [30], we include pixel blitting, geometric transformations, and color transforms in the augmentation pipeline. We additionally include cutout augmentation which works particularly well with our model, although it does not seem to have much effect on StyleGAN2. We also find it beneficial to apply color transforms less often and thus set their probability multiplier to 0.5 while retaining the multiplier 1 for other types of augmentations. As previously mentioned, we apply a fixed cosine schedule to the augmentation probability rather than adjusting it adaptively as in [30]. We did not observe any performance degradation with this simplification.

Network capacity. We keep the capacity distribution for each resolution the same as in [30, 32]. We place two residual blocks per resolution which makes our model roughly $3\times$ as deep, $1.5\text{--}3\times$ as wide as StyleGAN2 while maintaining the same model size on CIFAR-10 and FFHQ. For the ImageNet model, we double the number of channels which results in roughly $4\times$ as many parameters as the default StyleGAN2 configuration.

Mixed precision training. We apply mixed precision training as in [30, 32] where all parameters are stored in FP32, but cast to lower precision along with the activation maps for the 4 highest resolutions. We notice that using FP16 as the low precision format cripples the training of our model. However, we see no problem when using BFloat16 instead.

Class conditioning. For class conditional models, we follow the same conditioning scheme as in [30]. For G , the conditional latent code z' is the concatenation of z and the embedding of the class label c , specifically $z' = \text{concat}(z, \text{embed}(c))$. For D , we use a projection discriminator [54] which evaluates the dot product of the class embedding and the feature vector $D'(x)$ produced by the last layer of D , concretely $D(x) = \text{embed}(c) \cdot D'(x)^\top$. We do not employ any normalization-based conditioning such as AdaIN [29], AdaGN [7, 33], AdaBN [3] or AdaLN [58] for simplicity, even though they improve FID considerably.

Stacked MNIST. We base this model off of the CIFAR-10 model but without class conditioning. We disable all data augmentation and shorten the burn-in phase considerably. We use a constant learning rate and did not observe any benefit of using a lower learning rate later in the training.

Compute resources. We train the Stacked MNIST and CIFAR-10 models on an $8\times$ NVIDIA L40 node. Training took 7 hours for Stacked MNIST and 4 days for CIFAR-10. The FFHQ model was trained on an $8\times$ NVIDIA A6000 for roughly 3 weeks. The ImageNet model was trained on NVIDIA A100/H100 clusters and training took one day on 32 H100s (about 5000 H100 hours).

Hyperparameter	Stacked MNIST	CIFAR-10	FFHQ			ImageNet
Resolution	32×32	32×32	256×256	64×64	32×32	64×64
Class conditional	-	✓	-	-	✓	✓
Number of GPUs	8	8	8	8	32	64
Duration (Mimg)	10	250	200	100	1000	1000
Burn-in (Mimg)	2	20	20	20	200	200
Minibatch size	512	512	256	256	4096	4096
Learning rate	2×10^{-4}	$2 \times 10^{-4} \rightarrow 5 \times 10^{-5}$	$2 \times 10^{-4} \rightarrow 5 \times 10^{-5}$	$2 \times 10^{-4} \rightarrow 5 \times 10^{-5}$	$2 \times 10^{-4} \rightarrow 5 \times 10^{-5}$	$2 \times 10^{-4} \rightarrow 5 \times 10^{-5}$
γ for R_1 and R_2	$1 \rightarrow 0.1$	$0.05 \rightarrow 0.005$	$150 \rightarrow 15$	$2 \rightarrow 0.2$	$0.5 \rightarrow 0.05$	$1 \rightarrow 0.1$
Adam β_2	$0.9 \rightarrow 0.99$	$0.9 \rightarrow 0.99$	$0.9 \rightarrow 0.99$	$0.9 \rightarrow 0.99$	$0.9 \rightarrow 0.99$	$0.9 \rightarrow 0.99$
EMA half-life (Mimg)	$0 \rightarrow 0.5$	$0 \rightarrow 5$	$0 \rightarrow 0.5$	$0 \rightarrow 0.5$	$0 \rightarrow 50$	$0 \rightarrow 50$
Channels per resolution	768-768-768-768	768-768-768-768	96-192-384-768-768-768-768	384-768-768-768-768	1536-1536-1536-1536	1536-1536-1536-1536
ResBlocks per resolution	2-2-2-2	2-2-2-2	2-2-2-2-2-2-2	2-2-2-2-2	2-2-2-2	2-2-2-2-2
Groups per resolution	96-96-96-96	96-96-96-96	12-24-48-96-96-96-96	48-96-96-96-96	96-96-96-96	96-96-96-96-96
G params	20.73M	20.78M	23.06M	22.43M	82.91M	103.57M
D params	20.68M	21.28M	23.01M	22.38M	86.55M	107.21M
Dataset x -flips	-	✓	✓	✓	✓	✓
Augment probability	-	$0 \rightarrow 0.55$	$0 \rightarrow 0.3$	$0 \rightarrow 0.3$	$0 \rightarrow 0.5$	$0 \rightarrow 0.4$

Table 9: Hyperparameters for each experiment. The decay factor β of EMA can be obtained using the formula $\beta = 0.5^{\frac{\text{Minibatch size}}{\text{EMA half-life}}}$, e.g. for CIFAR-10, EMA $\beta = 0.5^{\frac{512}{5 \times 10^6}} \approx 0.9999$.

E Negative Results and Future Work

Following the convention of Brock *et al.* [3], we report alternative design choices that did not make to our final model. Either because they failed to produce any quantitative improvement or because they would considerably complicate our minimalist design which might be better suited for future study.

- We tried to apply GELU [18], Swish [61], and SMU [2] to G and D and found that doing so deteriorates FID considerably. We did not try on G xor D . We posit two independent factors:
 - ConvNeXt in general does not benefit much from GELU (and possibly similar activations). Table 10 and Table 11 in [48]: replacing ReLU with GELU gives little performance gain to ConvNeXt-T and virtually no performance gain to ConvNeXt-B.
 - In the context of GANs, GELU and Swish have the same problem as ReLU: that they have little gradient in the negative interval. Since G is updated from the gradient of D , having these activation functions in D could sparsify the gradient of D and as a result G will not receive as much useful information from D compared to using leaky ReLU.

This does not explain the strange case of SMU [2]: SMU is a smooth approximation of leaky ReLU and does not have the sparse gradient problem. It is unclear why it also underperformed and future work awaits.

- We tried adding group normalization [92] to G and D and it did not improve FID or training stability. We do not claim that all forms of normalizations are harmful. Our claim in principle c) only extends to normalization layers that explicitly standardizes the mean and standard deviation of the activation maps. This has been verified by prior studies [31, 34, 65]. The harm of normalization layers extends to the adjacent field of image restoration [43, 88]. To the best of our knowledge, EDM2 [34] is currently the strongest diffusion UNet and it does not use normalization layers. However, it does apply normalization to the trainable weights and this improves performance considerably. We expect that applying the normalization techniques in EDM2 would improve our model’s performance.
- We tried removing the activation function after the 3×3 grouped convolution in each residual block as modern architectures [48, 97] typically do not apply non-linearity after depthwise convolution. This worsened FID performance.
- We tried Pixel-Shuffle/Unshuffle [71] for changing the resolution of the activation maps, and found that without low-pass filtering, this led to high frequency artifacts similar to checkerboard artifacts even though Pixel-Shuffle does not have the uneven overlap problem that transposed convolution does. Note that bilinear resampling is equivalent to applying channel duplication/averaging with Pixel-Shuffle/Unshuffle in conjunction with a $[1, 2, 1]$ low-pass kernel. It might be interesting in future studies to explore inplace resampling filters that apply a low-pass filtered Pixel-Shuffle/Unshuffle operation on top of a learned function that changes the number of channels.
- We tried scaling up our model size. We found that allocating more model capacity to lower resolution stages generally did not improve FID, but contributed to more rapid overfitting. Increasing model capacity at higher resolution stages always improves FID in our experiments, however scaling up higher resolution stages is very computationally expensive. Capacity distribution for each resolution stage of the model might be an important topic to explore in future studies.
- For model simplicity, we did not conduct any experiment with a transformer architecture or attention mechanism in general. We are interested to see whether adding attention blocks to a convolutional network (similar to BigGAN [3] and diffusion UNet [20, 33, 34]) or using a pure transformer architecture (similar to DiT [58]) will result in stronger performance. Given the impressive results of EDM2 [34] (which uses UNet), it seems the argument has not yet settled for generative modeling.
- We experimented with Adam $\beta_2 = 0.999$ following common practice in supervised learning and diffusion models, and found that doing so led to stability issues on our ImageNet models. We expect that introducing proper normalization to our model will resolve this problem.
- We tried mixed precision training with IEEE FP16 as this is the low precision format used in StyleGAN2-ADA [30], StyleGAN3 [32], and EDM2 [34]. This crippled the training of

our model and switching to BFloat16 fixed the problem. We expect that introducing proper normalization to our model will allow us to use IEEE FP16 which offers more precision than BFloat16.

- We tried lazy regularization [31] in our early experiments where R_1 and R_2 were applied once every 8 minibatches. This led to slightly worse FID performance on real world datasets like FFHQ and CIFAR-10. However, it resulted in complete convergence failure on Stacked MNIST and several two dimensional toy datasets (line, circle, 25 Gaussians, *etc.*), indicating potential concerns regarding the mathematical legitimacy of this trick.

F Qualitative Results

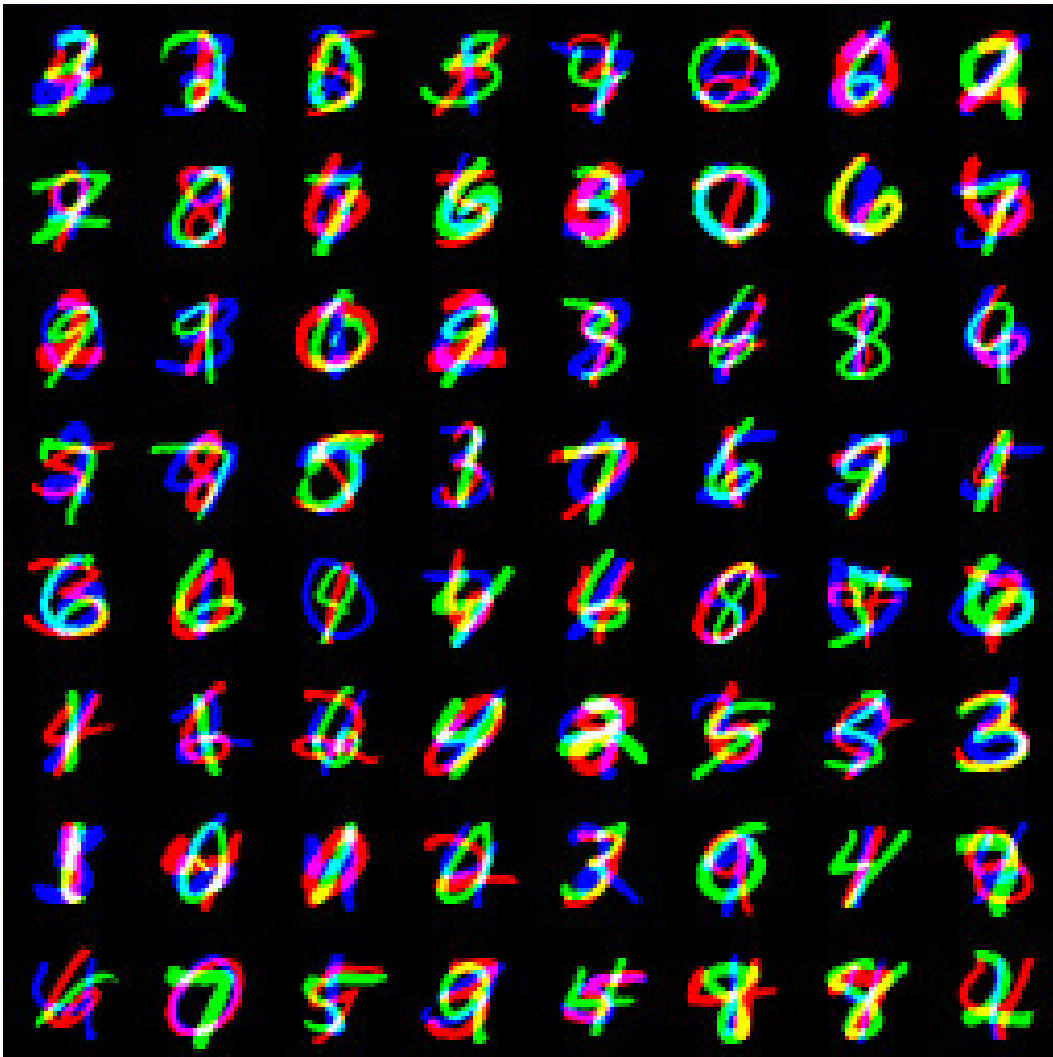


Figure 5: Qualitative examples of sample generation from our Config E on Stacked-MNIST.



Figure 6: More qualitative examples of sample generation from our Config E on FFHQ-256.

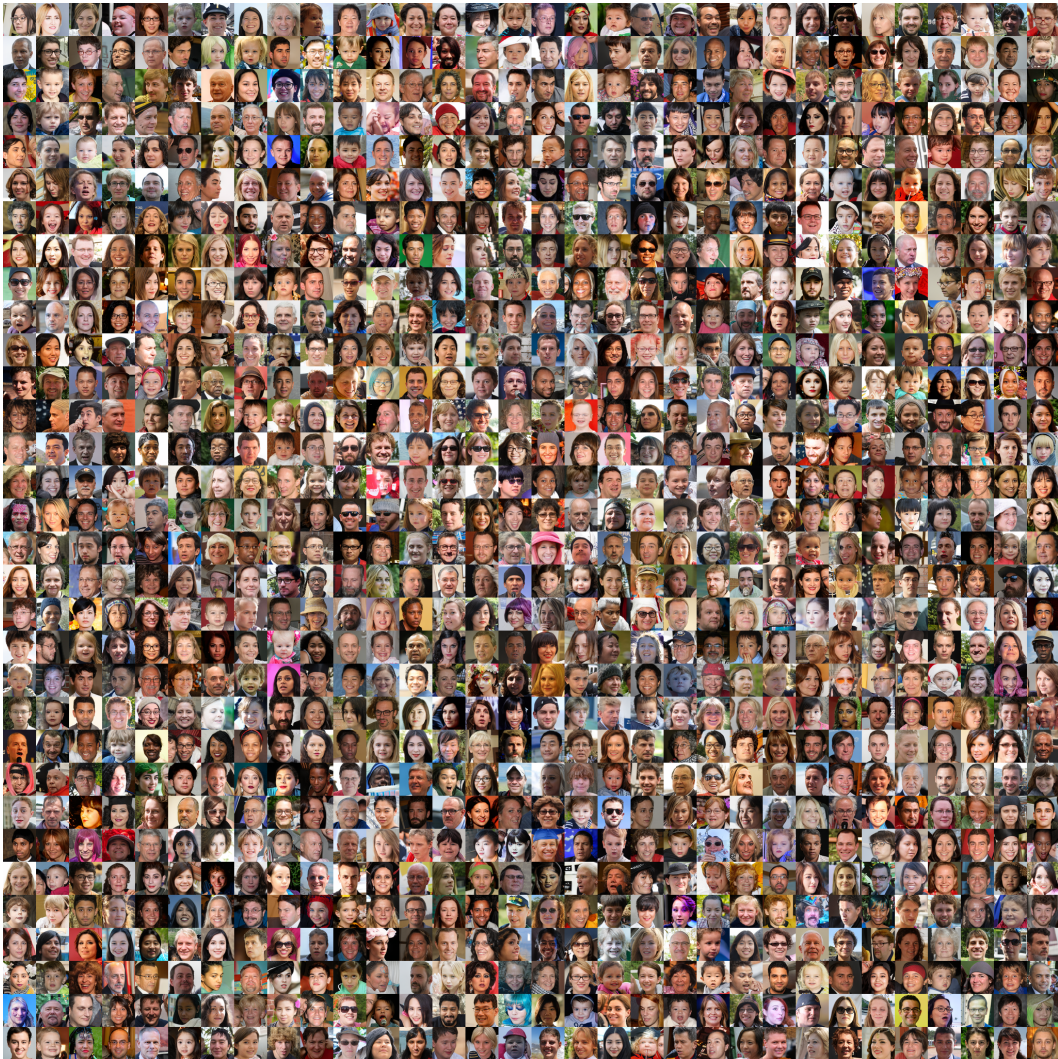


Figure 7: Qualitative examples of sample generation from our Config E on FFHQ-64.



Figure 8: Qualitative examples of sample generation from our Config E on CIFAR-10.



Figure 9: Qualitative examples of sample generation from our Config E on ImageNet-32.

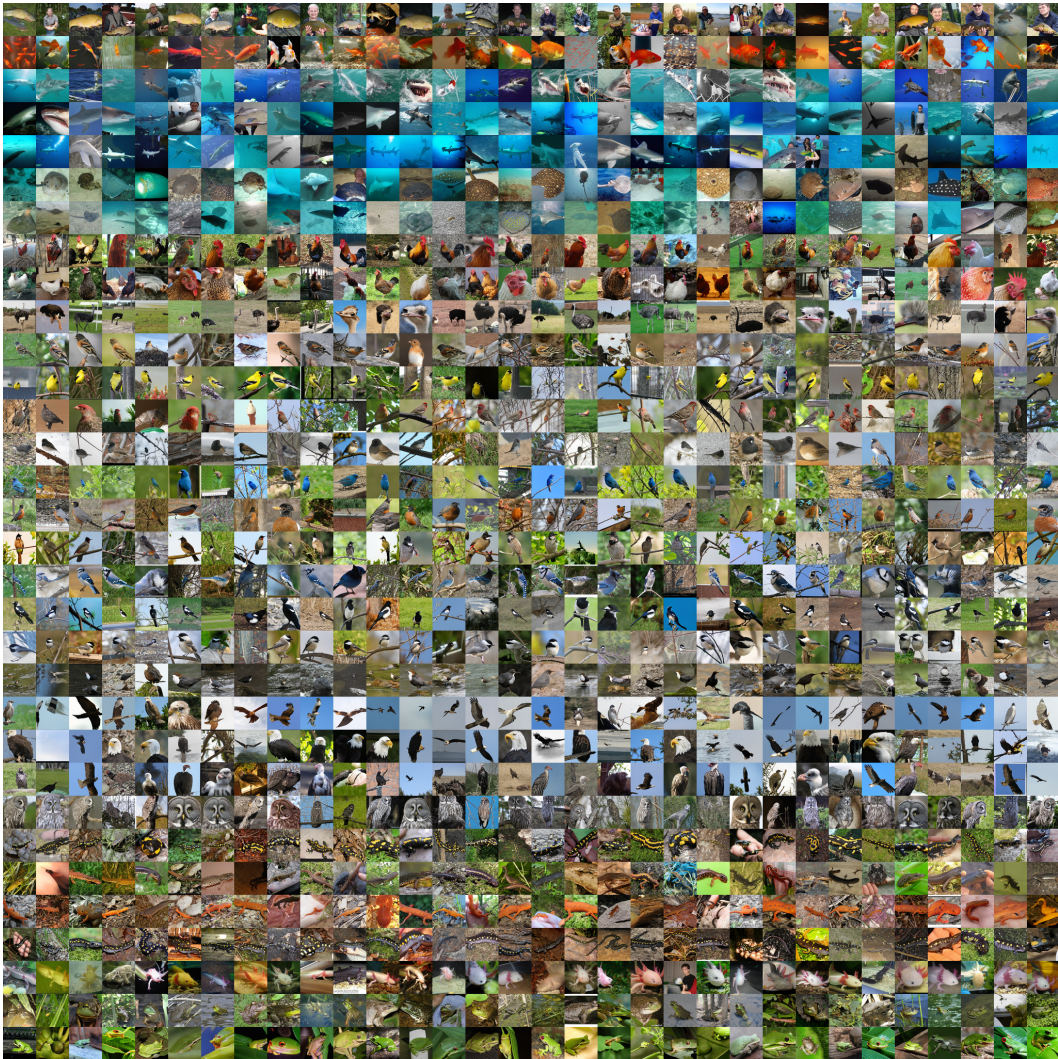


Figure 10: Qualitative examples of sample generation from our Config E on ImageNet-64.

G Training Curves

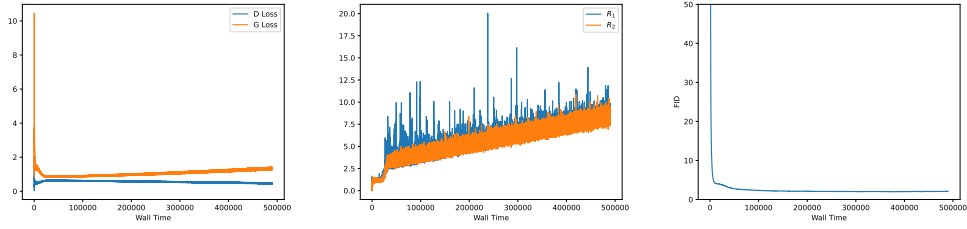


Figure 11: CIFAR-10 training curves.

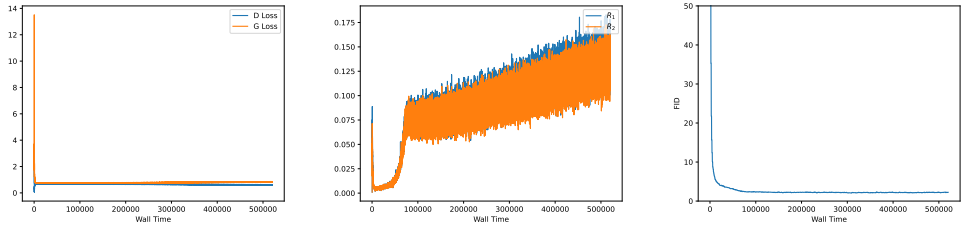


Figure 12: FFHQ-64 training curves.

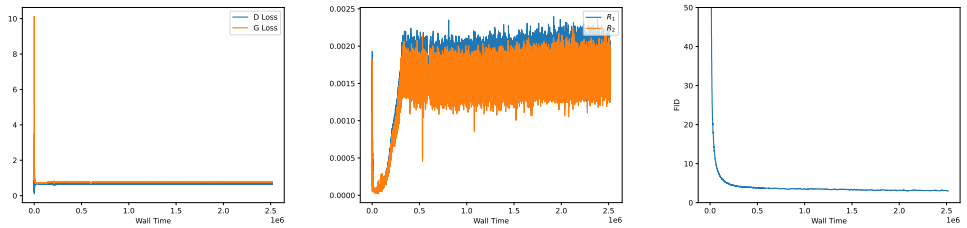


Figure 13: FFHQ-256 training curves.

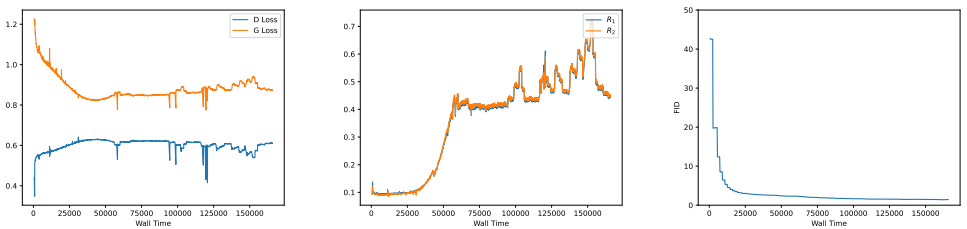


Figure 14: ImageNet-32 training curves.

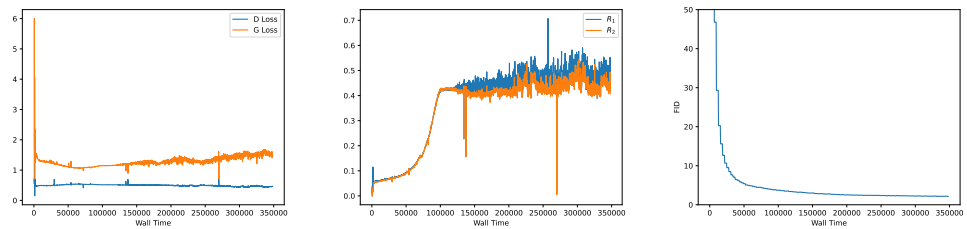


Figure 15: ImageNet-64 training curves.

NeurIPS Paper Checklist

1. Claims

Question: Do the main claims made in the abstract and introduction accurately reflect the paper's contributions and scope?

Answer: [Yes]

Justification: Claim of stability is justified by Figure 1 and later experimental performance. Claim of convergence properties is justified in Appendices A,B,C. Claim of SOTA GAN is experimentally justified in Section 4. Claims are bound to specific datasets.

Guidelines:

- The answer NA means that the abstract and introduction do not include the claims made in the paper.
- The abstract and/or introduction should clearly state the claims made, including the contributions made in the paper and important assumptions and limitations. A No or NA answer to this question will not be perceived well by the reviewers.
- The claims made should match theoretical and experimental results, and reflect how much the results can be expected to generalize to other settings.
- It is fine to include aspirational goals as motivation as long as it is clear that these goals are not attained by the paper.

2. Limitations

Question: Does the paper discuss the limitations of the work performed by the authors?

Answer: [Yes]

Justification: Please see Section 5.

Guidelines:

- The answer NA means that the paper has no limitation while the answer No means that the paper has limitations, but those are not discussed in the paper.
- The authors are encouraged to create a separate "Limitations" section in their paper.
- The paper should point out any strong assumptions and how robust the results are to violations of these assumptions (e.g., independence assumptions, noiseless settings, model well-specification, asymptotic approximations only holding locally). The authors should reflect on how these assumptions might be violated in practice and what the implications would be.
- The authors should reflect on the scope of the claims made, e.g., if the approach was only tested on a few datasets or with a few runs. In general, empirical results often depend on implicit assumptions, which should be articulated.
- The authors should reflect on the factors that influence the performance of the approach. For example, a facial recognition algorithm may perform poorly when image resolution is low or images are taken in low lighting. Or a speech-to-text system might not be used reliably to provide closed captions for online lectures because it fails to handle technical jargon.
- The authors should discuss the computational efficiency of the proposed algorithms and how they scale with dataset size.
- If applicable, the authors should discuss possible limitations of their approach to address problems of privacy and fairness.
- While the authors might fear that complete honesty about limitations might be used by reviewers as grounds for rejection, a worse outcome might be that reviewers discover limitations that aren't acknowledged in the paper. The authors should use their best judgment and recognize that individual actions in favor of transparency play an important role in developing norms that preserve the integrity of the community. Reviewers will be specifically instructed to not penalize honesty concerning limitations.

3. Theory Assumptions and Proofs

Question: For each theoretical result, does the paper provide the full set of assumptions and a complete (and correct) proof?

Answer: [Yes]

Justification: Prior knowledge of Mescheder *et al.* [52] is required, but this is cited appropriately to help the reader.

Guidelines:

- The answer NA means that the paper does not include theoretical results.
- All the theorems, formulas, and proofs in the paper should be numbered and cross-referenced.
- All assumptions should be clearly stated or referenced in the statement of any theorems.
- The proofs can either appear in the main paper or the supplemental material, but if they appear in the supplemental material, the authors are encouraged to provide a short proof sketch to provide intuition.
- Inversely, any informal proof provided in the core of the paper should be complemented by formal proofs provided in appendix or supplemental material.
- Theorems and Lemmas that the proof relies upon should be properly referenced.

4. Experimental Result Reproducibility

Question: Does the paper fully disclose all the information needed to reproduce the main experimental results of the paper to the extent that it affects the main claims and/or conclusions of the paper (regardless of whether the code and data are provided or not)?

Answer: [Yes]

Justification: Supplemental table lists all hyperparameters, and a supplemental section describes the training configurations.

Guidelines:

- The answer NA means that the paper does not include experiments.
- If the paper includes experiments, a No answer to this question will not be perceived well by the reviewers: Making the paper reproducible is important, regardless of whether the code and data are provided or not.
- If the contribution is a dataset and/or model, the authors should describe the steps taken to make their results reproducible or verifiable.
- Depending on the contribution, reproducibility can be accomplished in various ways. For example, if the contribution is a novel architecture, describing the architecture fully might suffice, or if the contribution is a specific model and empirical evaluation, it may be necessary to either make it possible for others to replicate the model with the same dataset, or provide access to the model. In general, releasing code and data is often one good way to accomplish this, but reproducibility can also be provided via detailed instructions for how to replicate the results, access to a hosted model (e.g., in the case of a large language model), releasing of a model checkpoint, or other means that are appropriate to the research performed.
- While NeurIPS does not require releasing code, the conference does require all submissions to provide some reasonable avenue for reproducibility, which may depend on the nature of the contribution. For example
 - (a) If the contribution is primarily a new algorithm, the paper should make it clear how to reproduce that algorithm.
 - (b) If the contribution is primarily a new model architecture, the paper should describe the architecture clearly and fully.
 - (c) If the contribution is a new model (e.g., a large language model), then there should either be a way to access this model for reproducing the results or a way to reproduce the model (e.g., with an open-source dataset or instructions for how to construct the dataset).
 - (d) We recognize that reproducibility may be tricky in some cases, in which case authors are welcome to describe the particular way they provide for reproducibility. In the case of closed-source models, it may be that access to the model is limited in some way (e.g., to registered users), but it should be possible for other researchers to have some path to reproducing or verifying the results.

5. Open access to data and code

Question: Does the paper provide open access to the data and code, with sufficient instructions to faithfully reproduce the main experimental results, as described in supplemental material?

Answer: [No]

Justification: There is no new data. There is no code at submission time. The authors will aim to release this by publication time, with instructions to faithfully reproduce the experiments. Code URL is included in abstract.

Guidelines:

- The answer NA means that paper does not include experiments requiring code.
- Please see the NeurIPS code and data submission guidelines (<https://nips.cc/public/guides/CodeSubmissionPolicy>) for more details.
- While we encourage the release of code and data, we understand that this might not be possible, so “No” is an acceptable answer. Papers cannot be rejected simply for not including code, unless this is central to the contribution (e.g., for a new open-source benchmark).
- The instructions should contain the exact command and environment needed to run to reproduce the results. See the NeurIPS code and data submission guidelines (<https://nips.cc/public/guides/CodeSubmissionPolicy>) for more details.
- The authors should provide instructions on data access and preparation, including how to access the raw data, preprocessed data, intermediate data, and generated data, etc.
- The authors should provide scripts to reproduce all experimental results for the new proposed method and baselines. If only a subset of experiments are reproducible, they should state which ones are omitted from the script and why.
- At submission time, to preserve anonymity, the authors should release anonymized versions (if applicable).
- Providing as much information as possible in supplemental material (appended to the paper) is recommended, but including URLs to data and code is permitted.

6. Experimental Setting/Details

Question: Does the paper specify all the training and test details (e.g., data splits, hyperparameters, how they were chosen, type of optimizer, etc.) necessary to understand the results?

Answer: [Yes]

Justification: Supplemental table lists all hyperparameters, and a supplemental section describes the training configurations.

Guidelines:

- The answer NA means that the paper does not include experiments.
- The experimental setting should be presented in the core of the paper to a level of detail that is necessary to appreciate the results and make sense of them.
- The full details can be provided either with the code, in appendix, or as supplemental material.

7. Experiment Statistical Significance

Question: Does the paper report error bars suitably and correctly defined or other appropriate information about the statistical significance of the experiments?

Answer: [No]

Justification: Each experiment takes many days to compute, some take weeks. We do not have the compute time to provide variance bars on training executions.

Guidelines:

- The answer NA means that the paper does not include experiments.
- The authors should answer "Yes" if the results are accompanied by error bars, confidence intervals, or statistical significance tests, at least for the experiments that support the main claims of the paper.

- The factors of variability that the error bars are capturing should be clearly stated (for example, train/test split, initialization, random drawing of some parameter, or overall run with given experimental conditions).
- The method for calculating the error bars should be explained (closed form formula, call to a library function, bootstrap, etc.)
- The assumptions made should be given (e.g., Normally distributed errors).
- It should be clear whether the error bar is the standard deviation or the standard error of the mean.
- It is OK to report 1-sigma error bars, but one should state it. The authors should preferably report a 2-sigma error bar than state that they have a 96% CI, if the hypothesis of Normality of errors is not verified.
- For asymmetric distributions, the authors should be careful not to show in tables or figures symmetric error bars that would yield results that are out of range (e.g. negative error rates).
- If error bars are reported in tables or plots, The authors should explain in the text how they were calculated and reference the corresponding figures or tables in the text.

8. Experiments Compute Resources

Question: For each experiment, does the paper provide sufficient information on the computer resources (type of compute workers, memory, time of execution) needed to reproduce the experiments?

Answer: [Yes]

Justification: Please see supplemental section on the experimental setting.

Guidelines:

- The answer NA means that the paper does not include experiments.
- The paper should indicate the type of compute workers CPU or GPU, internal cluster, or cloud provider, including relevant memory and storage.
- The paper should provide the amount of compute required for each of the individual experimental runs as well as estimate the total compute.
- The paper should disclose whether the full research project required more compute than the experiments reported in the paper (e.g., preliminary or failed experiments that didn't make it into the paper).

9. Code Of Ethics

Question: Does the research conducted in the paper conform, in every respect, with the NeurIPS Code of Ethics <https://neurips.cc/public/EthicsGuidelines>?

Answer: [Yes]

Justification: Experimental settings are standard and within the norms of the community.

Guidelines:

- The answer NA means that the authors have not reviewed the NeurIPS Code of Ethics.
- If the authors answer No, they should explain the special circumstances that require a deviation from the Code of Ethics.
- The authors should make sure to preserve anonymity (e.g., if there is a special consideration due to laws or regulations in their jurisdiction).

10. Broader Impacts

Question: Does the paper discuss both potential positive societal impacts and negative societal impacts of the work performed?

Answer: [Yes]

Justification: We mention it briefly in Section 5. The paper describes a basic machine learning methodology, and so does not address a specific application with specific societal impacts. But, GANs do have potential social impact; it is clear that face generation has a significant impact (e.g., deep fakes) and our paper does use a face database for evaluation thanks to it being a community norm.

Guidelines:

- The answer NA means that there is no societal impact of the work performed.
- If the authors answer NA or No, they should explain why their work has no societal impact or why the paper does not address societal impact.
- Examples of negative societal impacts include potential malicious or unintended uses (e.g., disinformation, generating fake profiles, surveillance), fairness considerations (e.g., deployment of technologies that could make decisions that unfairly impact specific groups), privacy considerations, and security considerations.
- The conference expects that many papers will be foundational research and not tied to particular applications, let alone deployments. However, if there is a direct path to any negative applications, the authors should point it out. For example, it is legitimate to point out that an improvement in the quality of generative models could be used to generate deepfakes for disinformation. On the other hand, it is not needed to point out that a generic algorithm for optimizing neural networks could enable people to train models that generate Deepfakes faster.
- The authors should consider possible harms that could arise when the technology is being used as intended and functioning correctly, harms that could arise when the technology is being used as intended but gives incorrect results, and harms following from (intentional or unintentional) misuse of the technology.
- If there are negative societal impacts, the authors could also discuss possible mitigation strategies (e.g., gated release of models, providing defenses in addition to attacks, mechanisms for monitoring misuse, mechanisms to monitor how a system learns from feedback over time, improving the efficiency and accessibility of ML).

11. Safeguards

Question: Does the paper describe safeguards that have been put in place for responsible release of data or models that have a high risk for misuse (e.g., pretrained language models, image generators, or scraped datasets)?

Answer: [No]

Justification: There is no new data and much larger models produce higher fidelity images. The cost of training these large GANs is not prohibitive and is often done by hobbyists. As such, it is doubtful that these models will unlock any *new* capabilities for mis-use or dual-use.

Guidelines:

- The answer NA means that the paper poses no such risks.
- Released models that have a high risk for misuse or dual-use should be released with necessary safeguards to allow for controlled use of the model, for example by requiring that users adhere to usage guidelines or restrictions to access the model or implementing safety filters.
- Datasets that have been scraped from the Internet could pose safety risks. The authors should describe how they avoided releasing unsafe images.
- We recognize that providing effective safeguards is challenging, and many papers do not require this, but we encourage authors to take this into account and make a best faith effort.

12. Licenses for existing assets

Question: Are the creators or original owners of assets (e.g., code, data, models), used in the paper, properly credited and are the license and terms of use explicitly mentioned and properly respected?

Answer: [Yes]

Justification: All datasets are cited.

Guidelines:

- The answer NA means that the paper does not use existing assets.
- The authors should cite the original paper that produced the code package or dataset.

- The authors should state which version of the asset is used and, if possible, include a URL.
- The name of the license (e.g., CC-BY 4.0) should be included for each asset.
- For scraped data from a particular source (e.g., website), the copyright and terms of service of that source should be provided.
- If assets are released, the license, copyright information, and terms of use in the package should be provided. For popular datasets, paperswithcode.com/datasets has curated licenses for some datasets. Their licensing guide can help determine the license of a dataset.
- For existing datasets that are re-packaged, both the original license and the license of the derived asset (if it has changed) should be provided.
- If this information is not available online, the authors are encouraged to reach out to the asset's creators.

13. **New Assets**

Question: Are new assets introduced in the paper well documented and is the documentation provided alongside the assets?

Answer: [NA]

Justification: No new assets are released.

Guidelines:

- The answer NA means that the paper does not release new assets.
- Researchers should communicate the details of the dataset/code/model as part of their submissions via structured templates. This includes details about training, license, limitations, etc.
- The paper should discuss whether and how consent was obtained from people whose asset is used.
- At submission time, remember to anonymize your assets (if applicable). You can either create an anonymized URL or include an anonymized zip file.

14. **Crowdsourcing and Research with Human Subjects**

Question: For crowdsourcing experiments and research with human subjects, does the paper include the full text of instructions given to participants and screenshots, if applicable, as well as details about compensation (if any)?

Answer: [NA]

Justification: No human subjects are used and no crowdsourcing is used.

Guidelines:

- The answer NA means that the paper does not involve crowdsourcing nor research with human subjects.
- Including this information in the supplemental material is fine, but if the main contribution of the paper involves human subjects, then as much detail as possible should be included in the main paper.
- According to the NeurIPS Code of Ethics, workers involved in data collection, curation, or other labor should be paid at least the minimum wage in the country of the data collector.

15. **Institutional Review Board (IRB) Approvals or Equivalent for Research with Human Subjects**

Question: Does the paper describe potential risks incurred by study participants, whether such risks were disclosed to the subjects, and whether Institutional Review Board (IRB) approvals (or an equivalent approval/review based on the requirements of your country or institution) were obtained?

Answer: [NA]

Justification: No human subjects are used and no crowdsourcing is used.

Guidelines:

- The answer NA means that the paper does not involve crowdsourcing nor research with human subjects.
- Depending on the country in which research is conducted, IRB approval (or equivalent) may be required for any human subjects research. If you obtained IRB approval, you should clearly state this in the paper.
- We recognize that the procedures for this may vary significantly between institutions and locations, and we expect authors to adhere to the NeurIPS Code of Ethics and the guidelines for their institution.
- For initial submissions, do not include any information that would break anonymity (if applicable), such as the institution conducting the review.